

1 **SARS-CoV-2 transmission dynamics in South Africa and epidemiological characteristics of the**
2 **Omicron variant**

3 Wan Yang¹ and Jeffrey Shaman²

4 ¹Department of Epidemiology, ²Department of Environmental Health Sciences, Mailman School
5 of Public Health, Columbia University, New York, NY, USA

6 Correspondence to: wy2202@cumc.columbia.edu

7
8 **Abstract**

9 Within days of first detection, Omicron SARS-CoV-2 variant case numbers grew exponentially
10 and spread globally. To better understand variant epidemiological characteristics, we utilize a
11 model-inference system to reconstruct SARS-CoV-2 transmission dynamics in South Africa and
12 decompose novel variant transmissibility and immune erosion. Accounting for under-detection
13 of infection, infection seasonality, nonpharmaceutical interventions, and vaccination, we
14 estimate that the majority of South Africans had been infected by SARS-CoV-2 before the
15 Omicron wave. Based on findings for Gauteng province, Omicron is estimated 100.3% (95% CI:
16 74.8 - 140.4%) more transmissible than the ancestral SARS-CoV-2 and 36.5% (95% CI: 20.9 -
17 60.1%) more transmissible than Delta; in addition, Omicron erodes 63.7% (95% CI: 52.9 - 73.9%)
18 of the population immunity, accumulated from prior infections and vaccination, in Gauteng.
19

20 **Main text**

21 In late November, 2021, South African scientists and public health officials reported a new
22 SARS-CoV-2 variant, subsequently named Omicron.¹ Within days, SARS-CoV-2 cases due to
23 Omicron increased dramatically in several provinces in South Africa,² despite substantial prior
24 infection of the population during previous pandemic waves, including a large, recent Delta
25 wave. Concurrently, Omicron was detected in an increasing number of countries (89, as of
26 12/17/21; GISAID data³) and appeared to spread with unprecedented speed in several
27 European countries.^{4,5} Multiple laboratory studies have reported large reductions (~20-40x) in
28 neutralizing ability of convalescent sera and vaccinee sera against Omicron, suggesting this
29 variant is able to erode components of adaptive immunity.⁶⁻⁹ In addition, preliminary *in vitro*
30 and/or *ex vivo* studies indicate that Omicron replicates faster within host than the Delta SARS-
31 CoV-2 variant,^{8,10} which has been the predominant variant since mid 2021. Together, this early
32 epidemiological and laboratory evidence points to both immune erosion and increased
33 transmissibility of Omicron. However, the relative importance of these two quantities remains
34 unclear.
35

36 To better understand the epidemiological characteristics of Omicron, we utilize a model-
37 inference system similar to one developed for study of SARS-CoV-2 variants of concern (VOCs),
38 including the Beta variant.¹¹ We use this system first to reconstruct SARS-CoV-2 transmission

39 dynamics in each of the nine provinces in South Africa, accounting for under-detection of
40 infection, infection seasonality, implemented nonpharmaceutical interventions (NPIs), and
41 vaccination (see Methods). Overall, the model-inference system is able to fit weekly case and
42 death data in each province (Fig 1A and Fig S1). We further validated the model-inference
43 estimates using three independent datasets. First, we used serology data. We note that early in
44 the pandemic serology data may reflect underlying infection rates but later, due to waning
45 antibody titers and reinfection, likely underestimate infection. Compared to seroprevalence
46 measures taken at multiple time points in each province, our model estimated cumulative
47 infection rates roughly match corresponding serology measures and trends over time; as
48 expected, model estimates were higher than serology measures taken during later months (Fig
49 1B). Second, compared to hospital admission data, across the nine provinces, model estimated
50 infection numbers were well correlated with numbers of hospitalizations for all three initial
51 pandemic waves caused by the ancestral, Beta, and Delta variants, respectively ($r > .85$, Fig 1 C-
52 E). Third, model-estimated infection numbers were correlated with age-adjusted excess
53 mortality for both the ancestral and Delta wave, but not the Beta wave (Fig 1C and E, vs. Fig
54 1D). Overall, these comparisons indicate our model-inference estimates align with underlying
55 transmission dynamics.

56
57 Next, we use Gauteng – the province with the earliest surge of Omicron – as an example to
58 highlight pandemic dynamics in South Africa thus far and develop key model-inference
59 estimates (Fig 2 for Gauteng and Fig S 2-9 for each of the other eight provinces). Despite lower
60 cases per capita than many other countries, infection numbers in South Africa were likely much
61 higher due to under-detection. For Gauteng, the estimated infection-detection rate during the
62 first pandemic wave was 4.31% (95% CI: 2.53 - 8.75%), and increased slightly to 5.21% (95% CI:
63 2.94 - 9.47%) and 5.88% (95% CI: 3.40 - 11.32%) during the Beta and Delta waves, respectively
64 (Table S1). These estimates are in line with those reported elsewhere based on serology data
65 (e.g., 4.74% detection rate during the first wave¹²). Accounting for under-detection (Fig 2E), we
66 estimate that 34.99% (95% CI: 17.22 - 59.52%, Table S2) of the population in Gauteng were
67 infected during the first wave, predominantly during winter when more conducive climate
68 conditions and relaxed public health restrictions existed (see the estimated seasonal and
69 mobility trends, Fig 2A).

70
71 With the emergence of Beta, another 25.91% (95% CI: 14.26 - 45.91%) of the population in
72 Gauteng – including reinfections – is estimated to have been infected, even though the Beta
73 wave occurred during summer under less conducive climate conditions for transmission (Fig
74 2A). Consistent with laboratory studies showing low neutralizing ability of convalescent sera
75 against Beta,^{13,14} the model-inference system estimates a large increase in population
76 susceptibility with the surge of Beta (Fig 2D). In addition to this immune erosion, an increase in

77 transmissibility is also evident for Beta, after accounting for concurrent NPIs and infection
78 seasonality (Fig 2C). Notably, in contrast to the large fluctuation of the time-varying effective
79 reproduction number over time (R_t , Fig 2B), the transmissibility estimates are more stable and
80 reflect changes in variant-specific properties. Further, consistent with in-depth epidemiological
81 findings,¹⁵ the estimated overall infection-fatality risk was higher for Beta than Ancestral SARS-
82 CoV-2 (0.16% [95% CI: 0.09 - 0.28%] vs. 0.09% [95% CI: 0.05 - 0.18%], Fig 2F and Table S3; n.b.
83 these estimates are based on documented COVID-19 deaths and are likely underestimates).

84
85 With the introduction of Delta, a third pandemic wave occurred in Gauteng during the 2021
86 winter. The model-inference system estimates a 53.19% (95% CI: 27.61 - 91.87%) attack rate by
87 Delta, despite the large number of infections during the previous two waves. This large attack
88 rate was possible, due to the high transmissibility of Delta, as reported in multiple studies,¹⁶⁻²⁰
89 the more conducive winter transmission conditions (Fig 2A), and the immune erosion from
90 Delta relative to both the ancestral and Beta variants. Consistent with this finding, and in
91 particular the estimated immune erosion, studies have reported a 27.5% reinfection rate during
92 the Delta pandemic wave in Delhi, India²¹ and reduced ability of sera from Beta-infection
93 recoverees to neutralize Delta.^{22,23}

94
95 Due to these large pandemic waves, prior to the detection of Omicron in Gauteng, estimated
96 cumulative infection numbers surpassed the population size (Fig 3B), indicating the large
97 majority of the population had been infected and some more than once. With the rise of
98 Omicron, the model-inference system estimates a very large increase in population
99 susceptibility (Fig 2D), as well as an increase in transmissibility (Fig 2C); however, unlike
100 previous waves, the Omicron wave progresses much more quickly, peaking 2-3 weeks after
101 initiating marked exponential growth. These estimates suggest that several additional factors
102 may have also contributed to the observed dynamics, including changes to the infection-
103 detection rate (Fig 2E), a summer seasonality increasingly suppressing transmission as the wave
104 progresses (Fig 2A), as well as a slight change in population mobility suggesting potential
105 behavior changes (Fig 2A).

106
107 Across all nine provinces in South Africa, the pandemic timing and intensity varied (Fig 3 A-C).
108 In addition to Gauteng, high cumulative infection rates during the first three pandemic waves
109 are also estimated for Western Cape and Northern Cape (Fig 1 C-E, Fig 3B and Table S2).
110 Overall, all nine provinces likely experienced three large pandemic waves prior to the growth of
111 Omicron; estimated average cumulative infections ranged from 58% of the population in
112 Limpopo to 126% in Northern Cape (Fig 3B).

113

114 Combining these model-inference estimates during each wave in each province, we estimate
115 that Beta eroded immunity among 72.1% (95% CI: 52.8 - 88.6%) of individuals with prior
116 ancestral SARS-CoV-2 infection and was 38.5% (95% CI: 16.2 – 56.0%) more transmissible than
117 the ancestral SARS-CoV-2. These estimates for Beta are consistent across the nine provinces
118 (Fig 3D, 1st column), as well as with our previous estimates using national data for South
119 Africa.¹¹ In comparison, estimates for Delta vary across the nine provinces (Fig 3D, 2nd column),
120 given the more diverse population immune landscape among provinces after two pandemic
121 waves. Overall, we estimate that Delta eroded 32.5% (95% CI: 0 – 60.9%) of prior immunity
122 (gained from infection by ancestral SARS-CoV-2 and/or Beta, and/or vaccination) and was
123 38.3% (95% CI: 21.2 - 58.5%) more transmissible than the ancestral SARS-CoV-2.

124

125 For Omicron, based on three provinces with the earliest surges (i.e., Gauteng, North West, and
126 Western Cape), we estimate that this variant erodes 55.0% (95% CI: 40.9 - 71.4%) of immunity
127 due to all prior infections and vaccination. In addition, it is 92.2% (95% CI: 70.2 - 128.5%) more
128 transmissible than the ancestral SARS-CoV-2. Based on estimates for Gauteng alone, Omicron is
129 100.3% (95% CI: 74.8 - 140.4%) more transmissible than the ancestral SARS-CoV-2, and 36.5%
130 (95% CI: 20.9 - 60.1%) more transmissible than Delta; in addition, it erodes 63.7% (95% CI: 52.9
131 - 73.9%) of the population immunity, accumulated from prior infections and vaccination, in
132 Gauteng.

133

134 Using a comprehensive model-inference system, we have reconstructed the pandemic
135 dynamics in each of the nine provinces in South Africa. Estimated underlying infection rates (Fig
136 1B-E) and key parameters (e.g. infection-detection rate and infection-fatality risk) are in line
137 with independent epidemiological data and investigations. These detailed model-inference
138 estimates thus allow assessment of both the transmissibility and immune erosion potential of
139 Omicron, and help contextualization and interpretation of Omicron transmission dynamics in
140 places outside South Africa. We show that, prior to the rise of Omicron, in Gauteng, the large
141 majority of population had been infected by one or more SARS-CoV-2 variants (including the
142 ancestral virus, Beta, and Delta), suggesting a high rate of immune erosion by Omicron versus
143 most, if not all, prior SARS-CoV-2 variants and vaccines. Interestingly, preliminary laboratory
144 data show that only 1 of 8 Beta, 1 of 7 Delta, and 0 of 10 Alpha convalescent sera had 50%
145 neutralization titers (IC50) >1:16 for Omicron.⁹ Combining these laboratory data with our
146 estimates of infection rates suggests 11% of the population would have retained immunity
147 against Omicron from prior Beta and Delta infection (i.e., $1/8 \times 25.9\%$ attack rate by Beta + $1/7$
148 $\times 53.2\%$ attack rate by Delta). However, studies have reported retained neutralizing ability
149 against Omicron among recoverees additionally vaccinated with 2 doses of vaccine.^{7,9}
150 Assuming an 80% probability of prior infection among the ~25% of Gauteng who received at
151 least 1 vaccine dose (by the end of Nov 2021), another 20% of population would have gained

152 immunity against Omicron from infection plus vaccination. In combination, this simple
153 conversion suggests the remaining ~70% of the population would be susceptible to Omicron,
154 similar to our model estimates (Fig 2D). Given the challenge of jointly estimating population
155 susceptibility (needed for estimating both prior immunity and immune erosion) and
156 transmissibility, the consistency of our population susceptibility estimates with available
157 laboratory evidence indicates that our estimates of transmissibility are also sensible.

158
159 Population susceptibility may differ across locations depending upon prior exposure to different
160 SARS-CoV-2 variants and vaccination uptake. However, similar calculations can be made in
161 other countries and regions, given prior infection and vaccination rates, in order to gauge local
162 susceptibility. In combination with the increased transmissibility estimated here and other
163 location conditions (e.g., infection seasonality and implementation of NPIs), modeling can then
164 be used to better anticipate the course of the Omicron wave. Nonetheless, the ability of
165 Omicron to spread with unprecedented pace in a heavily infected and partially vaccinated
166 population should serve as an alert for prompt public health response. More fundamentally, it
167 is yet another indication of the need for a global effort for increased vaccination, recurrent
168 boosting, and the development and distribution of effective and safe therapeutics for all
169 populations around the world.

170

171 **METHODS**

172 **Data sources and processing**

173 We used reported COVID-19 case and mortality data to capture transmission dynamics,
174 weather data to estimate infection seasonality, mobility data to represent concurrent NPIs, and
175 vaccination data to account for changes in population susceptibility due to vaccination in the
176 model-inference system. Provincial level COVID-19 case, mortality, and vaccination data were
177 sourced from the Coronavirus COVID-19 (2019-nCoV) Data Repository for South Africa
178 (COVID19ZA).²⁴ Hourly surface station temperature and relative humidity came from the
179 Integrated Surface Dataset (ISD) maintained by the National Oceanic and Atmospheric
180 Administration (NOAA) and are accessible using the “stationary” R package.^{25,26} We computed
181 specific humidity using temperature and relative humidity per the Clausius-Clapeyron
182 equation.²⁷ We then aggregated these data for all weather stations in each province with
183 measurements since 2000 and calculated the average for each week of the year during 2000-
184 2020.

185

186 Mobility data were derived from Google Community Mobility Reports;²⁸ we aggregated all
187 business-related categories (i.e., retail and recreational, transit stations, and workplaces) in all
188 locations in each province to weekly intervals. For vaccination, provincial vaccination data from
189 the COVID19ZA data repository recorded the total number of vaccine doses administered over

190 time; to obtain a breakdown for numbers of partial (1 dose of mRNA vaccine) and full
 191 vaccinations (1 dose of Janssen vaccine or 2 doses of mRNA vaccine), separately, we used
 192 national vaccination data for South Africa from Our World in Data^{29,30} to apportion the doses
 193 each day. In addition, cumulative case data suggested 18,586 new cases on Nov 23, 2021,
 194 whereas the South Africa Department of Health reported 868.³¹ Thus, for Nov 23, 2021, we
 195 used linear interpolation to fill in estimates for each province on that day and then scaled the
 196 estimates such that they sum to 868.

197

198 **Model-inference system**

199 The model-inference system is based on our previous work estimating changes in
 200 transmissibility and immune erosion for SARS-CoV-2 VOCs including Alpha, Beta, Gamma, and
 201 Delta.^{11,32} Below we describe each component.

202

203 *Epidemic model*

204 The epidemic model follows an SEIRSV (susceptible-exposed-infectious-recovered-susceptible-
 205 vaccination) construct per Eqn 1:

206

$$\begin{cases}
 \frac{dS}{dt} = \frac{R}{L_t} - \frac{b_t e_t m_t \beta_t IS}{N} - \varepsilon - v_{1,t} - v_{2,t} \\
 \frac{dE}{dt} = \frac{b_t e_t m_t \beta_t IS}{N} - \frac{E}{Z_t} + \varepsilon \\
 \frac{dI}{dt} = \frac{E}{Z_t} - \frac{I}{D_t} \\
 \frac{dR}{dt} = \frac{I}{D_t} - \frac{R}{L_t} + v_{1,t} + v_{2,t}
 \end{cases}$$

208

209 where S, E, I, R are the number of susceptible, exposed (but not yet infectious), infectious, and
 210 recovered/immune/deceased individuals; N is the population size; and ε is the number of
 211 travel-imported infections. In addition, the model includes the following key components:

212

- 213 1) Virus-specific properties, including the time-varying variant-specific transmission rate β_t ,
- 214 latency period Z_t , infectious period D_t , and immunity period L_t . Note all parameters are
- 215 estimated for each week (t) as described below.
- 216 2) The impact of NPIs. Specifically, we use relative population mobility (see data above) to
- 217 adjust the transmission rate via the term m_t , as the overall impact of NPIs (e.g., reduction
- 218 in the time-varying effective reproduction number R_t) has been reported to be highly
- 219 correlated with population mobility during the COVID-19 pandemic.³³⁻³⁵ To further account
- 220 for potential changes in effectiveness, the model additionally includes a parameter, e_t , to
- 221 scale NPI effectiveness.

- 222 3) The impact of vaccination, via the terms $v_{1,t}$ and $v_{2,t}$. Specifically, $v_{1,t}$ is the number of
223 individuals successfully immunized after the first dose of vaccine and is computed using
224 vaccination data and vaccine effectiveness (VE) for 1st dose; and $v_{2,t}$ is the additional
225 number of individuals successfully immunized after the second vaccine dose (i.e., excluding
226 those successfully immunized after the first dose). In South Africa, around two-thirds of
227 vaccines administered during our study period were the mRNA BioNTech/Pfizer vaccine
228 and one-third the Janssen vaccine.³⁶ We thus set VE to 20%/85% (partial/full vaccination)
229 for Beta, 35%/75% for Delta, and 10%/35% for Omicron based on reported VE estimates.³⁷⁻
230³⁹
- 231 4) Infection seasonality, computed using temperature and specific humidity data as described
232 previously (see supplemental material of Yang and Shaman¹¹). Briefly, we estimated the
233 relative seasonal trend (b_t) using a model representing the dependency of the survival of
234 respiratory viruses including SARS-CoV-2 to temperature and humidity.^{40,41} As shown in Fig
235 2A, b_t estimates over the year averaged to 1 such that weeks with $b_t > 1$ (e.g. during the
236 winter) are more conducive to SARS-CoV-2 transmission whereas weeks with $b_t < 1$ (e.g.
237 during the summer) have less favorable climate conditions for transmission. The estimated
238 relative seasonal trend, b_t , is used to adjust the relative transmission rate at time t in Eqn 1.
239

240 *Observation model to account for under-detection and delay*

241 Using the model-simulated number of infections occurring each day, we further computed the
242 number of cases and deaths each week to match with the observations, as done in Yang et al.⁴²
243 Briefly, we include 1) a time-lag from infectiousness to detection (i.e., an infection being
244 diagnosed as a case), drawn from a gamma distribution with a mean of $T_{d,mean}$ days and a
245 standard deviation of $T_{d,sd}$ days, to account for delays in detection (Table S4); 2) an infection-
246 detection rate (r_t), i.e. the fraction of infections (including subclinical or asymptomatic
247 infections) reported as cases, to account for under-detection; 3) a time-lag from infectiousness
248 to death, drawn from a gamma distribution with a mean of 13-15 days and a standard deviation
249 of 10 days; and 4) an infection-fatality risk (IFR_t). To compute the model-simulated number of
250 new cases each week, we multiplied the model-simulated number of new infections per day by
251 the infection-detection rate, and further distributed these simulated cases in time per the
252 distribution of time-from-infectiousness-to-detection. Similarly, to compute the model-
253 simulated deaths per week and account for delays in time to death, we multiplied the
254 simulated-infections by the IFR and then distributed these simulated deaths in time per the
255 distribution of time-from-infectious-to-death. We then aggregated these daily numbers to
256 weekly totals to match with the weekly case and mortality data for model-inference. For each
257 week, the infection-detection rate (r_t), the infection-fatality risk (IFR_t), and the two time-to-
258 detection parameters ($T_{d,mean}$ and $T_{d,sd}$) were estimated along with other parameters (see
259 below).

260

261 *Model inference and parameter estimation*

262 The inference system uses the ensemble adjustment Kalman filter, EAKF,⁴³ a Bayesian statistical
263 method, to estimate model state variables (i.e., S, E, I, R from Eqn 1) and parameters (i.e., $\beta_t, Z_t,$
264 $D_t, L_t, e_t,$ from Eqn 1 as well as r_t, IFR_t and other parameters from the observation model).
265 Briefly, the EAKF uses an ensemble of model realizations ($n=500$ here), each with initial
266 parameters and variables randomly drawn from a *prior* range (see Table S4). After model
267 initialization, the system integrates the model ensemble forward in time for a week (per Eqn 1)
268 to compute the prior distribution for each model state variable and parameter, as well as the
269 model-simulated number of cases and deaths for that week. The system then combines the
270 prior estimates with the observed case and death data for the same week to compute the
271 posterior per Bayes' theorem.⁴³ During this filtering process, the system updates the posterior
272 distribution of all model variables and parameters for each week.

273

274 *Estimating changes in transmissibility and immune erosion for each variant*

275 As in ref¹¹, we computed the variant-specific transmissibility (R_{TX}) as the product of the
276 variant-specific transmission rate (β_t) and infectious period (D_t). Note that R_t , the time-varying
277 effective reproduction number, is defined as $R_t = b_t e_t m_t \beta_t D_t S/N = b_t e_t m_t R_{TX} S/N$. To
278 reduce uncertainty, we averaged transmissibility estimates over the period a particular variant
279 of interest was predominant. To find these predominant periods, we first specified the
280 approximate timing of each pandemic wave in each province based on: 1) when available,
281 genomic surveillance data; specifically, the onsets of the Beta wave in Eastern Cape, Western
282 Cape, KwaZulu-Natal, and Northern Cape, were separately based on the initial detection of Beta
283 in these provinces as reported in Tegally et al;⁴⁴ the onsets of the Delta wave in each of the nine
284 provinces, separately, were based on genomic sequencing data from the Network for Genomic
285 Surveillance South Africa (NGS-SA);⁴⁵ and 2) when genomic data were not available, we used
286 the week with the lowest case number between two waves. The specified calendar periods are
287 listed in Table S5. During later waves, multiple variants could initially co-circulate before one
288 became predominant. As a result, the estimated transmissibility tended to increase before
289 reaching a plateau (see, e.g., Fig 2C). In addition, in a previous study of the Delta pandemic
290 wave in India,³² we also observed that when many had been infected, transmissibility could
291 decrease a couple months after the peak, likely due to increased reinfections for which onward
292 transmission may be reduced. Thus, to obtain a more variant-specific estimate, we computed
293 the average transmissibility ($\overline{R_{TX}}$) using the weekly R_{TX} estimates over the 8-week period
294 starting the week prior to the maximal R_{TX} during each wave; if no maximum existed (e.g. when
295 a new variant is less transmissible), we simply averaged over the entire wave. We then

296 computed the change in transmissibility due to a given variant relative to the ancestral SARS-
297 CoV-2 as $(\frac{R_{TX,variant} - R_{TX,ancestral}}{R_{TX,ancestral}}) \times 100\%$.

298
299 To quantify immune erosion, similar to ref¹¹, we estimated changes in susceptibility over time
300 and computed the change in immunity as $\Delta Imm = S_{t+1} - S_t + i_t$, where S_t is the susceptibility at
301 time- t and i_t is the new infections occurring during each week- t . We sum over all ΔImm
302 estimates for a particular location, during each wave, to compute the total change in immunity
303 due to a new variant, $\Sigma \Delta Imm_v$. We then computed the level of immune erosion as the ratio of
304 $\Sigma \Delta Imm_v$ to the model-estimated population immunity prior to the first detection of immune
305 erosion, during each wave. That is, as opposed to having a common reference of prior
306 immunity, here immune erosion for each variant depends on the state of the population
307 immune landscape – i.e., combining all prior exposures and vaccinations – immediately
308 preceding the surge of that variant.

309
310 For all provinces, model-inference was initiated the week starting March 15, 2020 and run
311 continuously until the week starting Dec 12, 2021. To account for model stochasticity, we
312 repeated the model-inference process 100 times for each province, each with 500 model
313 realizations and summarized the results from all 50,000 model estimates.

314 315 **Model validation using independent data**

316 To compare model estimates with independent observations not assimilated into the model-
317 inference system, we utilized three relevant datasets:

- 318
- 319 1) Serological survey data measuring the prevalence of SARS-CoV-2 antibodies over time.
320 Multiple serology surveys have been conducted in different provinces of South Africa. The
321 South African COVID-19 Modelling Consortium summarizes the findings from several of
322 these surveys (see Fig 1A of ref⁴⁶). We digitized all data presented in Fig 1A of ref⁴⁶ and
323 compared these to corresponding model-estimated cumulative infection rates (computed
324 mid-month for each corresponding month with a seroprevalence measure). Due to
325 unknown survey methodologies and challenges adjusting for sero-reversion and
326 reinfection, we used these data directly (i.e., without adjustment) for qualitative
327 comparison.
 - 328 2) COVID-19-related hospitalization data, from COVID19ZA.²⁴ We aggregated the total
329 number of COVID-19 hospital admissions during each wave and compared these
330 aggregates to model-estimated cumulative infection rates during the same wave. Of note,
331 these hospitalization data were available from June 6, 2020 onwards and are thus
332 incomplete for the first wave.

333 3) Age-adjusted excess mortality data from the South African Medical Research Council
334 (SAMRC).⁴⁷ Deaths due to COVID-19 (used in the model-inference system) are
335 undercounted. Thus, we also compared model-estimated cumulative infection rates to age-
336 adjusted excess mortality data during each wave. Of note, excess mortality data were
337 available from May 3, 2020 onwards and are thus incomplete for the first wave.

338
339
340 **Data Availability:** All data used in this study are publicly available as described in the “Data
341 sources and processing” section.

342
343 **Code availability:** All source code and data necessary for the replication of our results and
344 figures will be made publicly available on Github.

345
346 **Acknowledgements:** This study was supported by the National Institute of Allergy and
347 Infectious Diseases (AI145883 and AI163023), the Centers for Disease Control and Prevention
348 (CK000592), and a gift from the Morris-Singer Foundation.

349
350 **Author contributions:** WY designed the study (main), conducted the model analyses,
351 interpreted results, and wrote the first draft. JS designed the study (supporting), interpreted
352 results, and critically revised the manuscript.

353
354 **Competing interests:** JS and Columbia University disclose partial ownership of SK Analytics. JS
355 discloses consulting for BNI.

356
357 **References:**

- 358 1 World Health Organization. Classification of Omicron (B.1.1.529): SARS-CoV-2 Variant of
359 Concern. (2021).
- 360 2 Viana et al. *Rapid epidemic expansion of the SARS-CoV-2 Omicron variant in southern*
361 *Africa*, <[https://krisp.org.za/manuscripts/ZHTOWa-MEDRXIV-2021-268028v1-](https://krisp.org.za/manuscripts/ZHTOWa-MEDRXIV-2021-268028v1-deOliveira.pdf)
362 [deOliveira.pdf](https://krisp.org.za/manuscripts/ZHTOWa-MEDRXIV-2021-268028v1-deOliveira.pdf)> (2021).
- 363 3 Global Initiative on Sharing All Influenza Data (GISAID). *Tracking of Variants*,
364 <<https://www.gisaid.org/hcov19-variants/>> (2021).
- 365 4 UK Health Security Agency. Omicron daily overview: 17 December 2021. (2021).
- 366 5 Espenhain, L. *et al.* Epidemiological characterisation of the first 785 SARS-CoV-2
367 Omicron variant cases in Denmark, December 2021. *Eurosurveillance* **26**, 2101146,
368 doi:doi:<https://doi.org/10.2807/1560-7917.ES.2021.26.50.2101146> (2021).
- 369 6 Nemet, I. *et al.* Third BNT162b2 vaccination neutralization of SARS-CoV-2 Omicron
370 infection. *medRxiv*, 2021.2012.2013.21267670, doi:10.1101/2021.12.13.21267670
371 (2021).

372 7 Cele, S. *et al.* SARS-CoV-2 Omicron has extensive but incomplete escape of Pfizer
373 BNT162b2 elicited neutralization and requires ACE2 for infection. *medRxiv*,
374 2021.2012.2008.21267417, doi:10.1101/2021.12.08.21267417 (2021).

375 8 Garcia-Beltran, W. F. *et al.* mRNA-based COVID-19 vaccine boosters induce neutralizing
376 immunity against SARS-CoV-2 Omicron variant. *medRxiv*, 2021.2012.2014.21267755,
377 doi:10.1101/2021.12.14.21267755 (2021).

378 9 Rössler, A., Riepler, L., Bante, D., Laer, D. v. & Kimpel, J. SARS-CoV-2 B.1.1.529 variant
379 (Omicron) evades neutralization by sera from vaccinated and convalescent individuals.
380 *medRxiv*, 2021.2012.2008.21267491, doi:10.1101/2021.12.08.21267491 (2021).

381 10 Li Ka Shing Faculty of Medicine. *HKUMed finds Omicron SARS-CoV-2 can infect faster and*
382 *better than Delta in human bronchus but with less severe infection in lung*, 2021).

383 11 Yang, W. & Shaman, J. Development of a model-inference system for estimating
384 epidemiological characteristics of SARS-CoV-2 variants of concern. *Nature*
385 *Communications* **12**, 5573, doi:<https://doi.org/10.1038/s41467-021-25913-9> (2021).

386 12 Kleynhans, J. *et al.* SARS-CoV-2 Seroprevalence in a Rural and Urban Household Cohort
387 during First and Second Waves of Infections, South Africa, July 2020-March 2021. *Emerg*
388 *Infect Dis* **27**, 3020-3029, doi:10.3201/eid2712.211465 (2021).

389 13 Garcia-Beltran, W. F. *et al.* Multiple SARS-CoV-2 variants escape neutralization by
390 vaccine-induced humoral immunity. *Cell* **184**, 2372-2383 e2379,
391 doi:10.1016/j.cell.2021.03.013 (2021).

392 14 Wall, E. C. *et al.* Neutralising antibody activity against SARS-CoV-2 VOCs B.1.617.2 and
393 B.1.351 by BNT162b2 vaccination. *Lancet*, doi:10.1016/S0140-6736(21)01290-3 (2021).

394 15 Abu-Raddad, L. J. *et al.* Severity, Criticality, and Fatality of the Severe Acute Respiratory
395 Syndrome Coronavirus 2 (SARS-CoV-2) Beta Variant. *Clinical Infectious Diseases*,
396 doi:10.1093/cid/ciab909 (2021).

397 16 Public Health England. *SARS-CoV-2 variants of concern and variants under investigation*
398 *in England. Technical briefing 14*,
399 [https://assets.publishing.service.gov.uk/government/uploads/system/uploads/attach](https://assets.publishing.service.gov.uk/government/uploads/system/uploads/attachment_data/file/991343/Variants_of_Concern_VOC_Technical_Briefing_14.pdf)
400 [ment_data/file/991343/Variants of Concern VOC Technical Briefing 14.pdf](https://assets.publishing.service.gov.uk/government/uploads/system/uploads/attachment_data/file/991343/Variants_of_Concern_VOC_Technical_Briefing_14.pdf)> (2021).

401 17 Allen, H. *et al.* Household transmission of COVID-19 cases associated with SARS-CoV-2
402 delta variant (B.1.617.2): national case-control study. *The Lancet regional health.*
403 *Europe*, 100252, doi:10.1016/j.lanepe.2021.100252 (2021).

404 18 Challen, R. *et al.* Early epidemiological signatures of novel SARS-CoV-2 variants:
405 establishment of B.1.617.2 in England. *medRxiv*, 2021.2006.2005.21258365,
406 doi:10.1101/2021.06.05.21258365 (2021).

407 19 Earnest, R. *et al.* Comparative transmissibility of SARS-CoV-2 variants Delta and Alpha in
408 New England, USA. *medRxiv*, doi:10.1101/2021.10.06.21264641 (2021).

409 20 Vohringer, H. S. *et al.* Genomic reconstruction of the SARS-CoV-2 epidemic in England.
410 *Nature*, doi:10.1038/s41586-021-04069-y (2021).

411 21 Dhar, M. S. *et al.* Genomic characterization and epidemiology of an emerging SARS-CoV-
412 2 variant in Delhi, India. *Science*, eabj9932, doi:10.1126/science.abj9932 (2021).

413 22 Liu, C. *et al.* Reduced neutralization of SARS-CoV-2 B.1.617 by vaccine and convalescent
414 serum. *Cell* **184**, 4220+, doi:10.1016/j.cell.2021.06.020 (2021).

415 23 de Oliveira, T. & Lessells, R. *Update on Delta and other variants in South Africa and other*
416 *world*, <[https://www.krisp.org.za/manuscripts/DeltaGammaSummary_NGS-](https://www.krisp.org.za/manuscripts/DeltaGammaSummary_NGS-SA_6JulV2.pdf)
417 [SA_6JulV2.pdf](https://www.krisp.org.za/manuscripts/DeltaGammaSummary_NGS-SA_6JulV2.pdf)> (2021).

418 24 Data Science for Social Impact Research Group at University of Pretoria. *Coronavirus*
419 *COVID-19 (2019-nCoV) Data Repository for South Africa*,
420 <<https://github.com/dsfsi/covid19za>> (2021).

421 25 Iannone, R. *Package 'stationaRy'*, <[https://cran.r-](https://cran.r-project.org/web/packages/stationaRy/stationaRy.pdf)
422 [project.org/web/packages/stationaRy/stationaRy.pdf](https://cran.r-project.org/web/packages/stationaRy/stationaRy.pdf)> (2020).

423 26 Iannone, R. *stationaRy*, <<https://github.com/rich-iannone/stationaRy>> (2020).

424 27 Wallace, J. & Hobbs, P. *Atmospheric Science: An Introductory survey*. 2nd Edition edn,
425 (Academic Press, 2006).

426 28 Google Inc. *Community Mobility Reports*, <<https://www.google.com/covid19/mobility/>>
427 (2020).

428 29 *Data on COVID-19 (coronavirus) vaccinations by Our World in Data*,
429 <<https://github.com/owid/covid-19-data/tree/master/public/data/vaccinations>> (2020).

430 30 Mathieu, E. *et al.* A global database of COVID-19 vaccinations. *Nat Hum Behav* **5**, 947-
431 953, doi:10.1038/s41562-021-01122-8 (2021).

432 31 Department of Health Republic of South Africa. *Update on Covid-19 (Tuesday 23*
433 *November 2021)*, <[https://sacoronavirus.co.za/2021/11/23/update-on-covid-19-](https://sacoronavirus.co.za/2021/11/23/update-on-covid-19-tuesday-23-november-2021/)
434 [tuesday-23-november-2021/](https://sacoronavirus.co.za/2021/11/23/update-on-covid-19-tuesday-23-november-2021/)> (2021).

435 32 Yang, W. & Shaman, J. COVID-19 pandemic dynamics in India, the SARS-CoV-2 Delta
436 variant, and implications for vaccination. *medRxiv*, 2021.2006.2021.21259268,
437 doi:10.1101/2021.06.21.21259268 (2021).

438 33 Yang, W., Shaff, J. & Shaman, J. Effectiveness of non-pharmaceutical interventions to
439 contain COVID-19: a case study of the 2020 spring pandemic wave in New York City. *J R*
440 *Soc Interface* **18**, 20200822, doi:10.1098/rsif.2020.0822 (2021).

441 34 Lasry, A. *et al.* Timing of Community Mitigation and Changes in Reported COVID-19 and
442 Community Mobility - Four U.S. Metropolitan Areas, February 26-April 1, 2020. *MMWR.*
443 *Morbidity and mortality weekly report* **69**, 451-457, doi:10.15585/mmwr.mm6915e2
444 (2020).

445 35 Kraemer, M. U. G. *et al.* The effect of human mobility and control measures on the
446 COVID-19 epidemic in China. *Science* **368**, 493-497, doi:10.1126/science.abb4218
447 (2020).

448 36 Department of Health Republic of South Africa. *Latest Vaccine Statistics*,
449 <<https://sacoronavirus.co.za/latest-vaccine-statistics/>> (2021).

450 37 Abu-Raddad, L. J., Chemaitelly, H. & Butt, A. A. Effectiveness of the BNT162b2 Covid-19
451 Vaccine against the B.1.1.7 and B.1.351 Variants. *New Engl J Med*,
452 doi:10.1056/NEJMc2104974 (2021).

453 38 Bernal, J. L. *et al.* Effectiveness of Covid-19 Vaccines against the B.1.617.2 (Delta)
454 Variant. *New England Journal of Medicine* **385**, 585-594, doi:10.1056/NEJMoa2108891
455 (2021).

456 39 Andrews, N. *et al.* Effectiveness of COVID-19 vaccines against the Omicron (B.1.1.529)
457 variant of concern. *medRxiv*, 2021.2012.2014.21267615,
458 doi:10.1101/2021.12.14.21267615 (2021).

459 40 Biryukov, J. *et al.* Increasing Temperature and Relative Humidity Accelerates Inactivation
460 of SARS-CoV-2 on Surfaces. *mSphere* **5**, e00441-00420, doi:doi:10.1128/mSphere.00441-
461 20 (2020).

462 41 Morris, D. H. *et al.* Mechanistic theory predicts the effects of temperature and humidity
463 on inactivation of SARS-CoV-2 and other enveloped viruses. *Elife* **10**,
464 doi:10.7554/eLife.65902 (2021).

465 42 Yang, W. *et al.* Estimating the infection-fatality risk of SARS-CoV-2 in New York City
466 during the spring 2020 pandemic wave: a model-based analysis. *The Lancet. Infectious*
467 *diseases* **21**, 203-212, doi:10.1016/S1473-3099(20)30769-6 (2021).

468 43 Anderson, J. L. An ensemble adjustment Kalman filter for data assimilation. *Mon.*
469 *Weather Rev.* **129**, 2884-2903, doi:Doi 10.1175/1520-
470 0493(2001)129<2884:Aeakff>2.0.Co;2 (2001).

471 44 Tegally, H. *et al.* Detection of a SARS-CoV-2 variant of concern in South Africa. *Nature*
472 **592**, 438-443, doi:10.1038/s41586-021-03402-9 (2021).

473 45 The National Institute for Communicable Diseases (NICD) of the National Health
474 Laboratory (NHLS) on behalf of the Network for Genomics Surveillance in South Africa
475 (NGS-SA). *Network for Genomic Surveillance South Africa (NGS-SA) SARS-CoV-2*
476 *Sequencing Update 19 August 2021*, < [https://www.nicd.ac.za/wp-](https://www.nicd.ac.za/wp-content/uploads/2021/08/Update-of-SA-sequencing-data-from-GISAID-19-August-2021.pdf)
477 [content/uploads/2021/08/Update-of-SA-sequencing-data-from-GISAID-19-August-](https://www.nicd.ac.za/wp-content/uploads/2021/08/Update-of-SA-sequencing-data-from-GISAID-19-August-2021.pdf)
478 [2021.pdf](https://www.nicd.ac.za/wp-content/uploads/2021/08/Update-of-SA-sequencing-data-from-GISAID-19-August-2021.pdf)> (2021).

479 46 The South African COVID-19 Modelling Consortium. *COVID-19 modelling update:*
480 *Considerations for a potential fourth wave (17 Nov 2021)*, <[https://www.nicd.ac.za/wp-](https://www.nicd.ac.za/wp-content/uploads/2021/11/SACMC-Fourth-wave-report-17112021-final.pdf)
481 [content/uploads/2021/11/SACMC-Fourth-wave-report-17112021-final.pdf](https://www.nicd.ac.za/wp-content/uploads/2021/11/SACMC-Fourth-wave-report-17112021-final.pdf)> (2021).

482 47 The South African Medical Research Council (SAMRC). *Report on Weekly Deaths in South*
483 *Africa*, <<https://www.samrc.ac.za/reports/report-weekly-deaths-south-africa>> (2021).
484

Fig 1. Pandemic dynamics in South Africa, model-fit and validation using independent data.

(A) Pandemic dynamics in each of the nine provinces (see legend); dots depict reported weekly numbers of cases and deaths; lines show model mean estimates (in the same color). For validation, model estimated infection rates are compared to seroprevalence measures over time from multiple sero-surveys summarized in ref¹ (B), COVID-related hospitalizations (left panel) and age-adjusted excess mortality (right panel) during the Ancestral (C), Beta (D), and Delta (E) waves. Boxplots depict the estimated distribution for each province (middle bar = mean; edges = 50% Crls) and whiskers (95% Crls). Red dots show corresponding measurements. Correlation (r) between model estimated cumulative infection rate and cumulative hospitalization or age-adjusted excess mortality (C-E) for each wave is shown in each plot. *Note that hospitalization data begin from 6/6/20 and excess mortality data begin from 5/3/20 and thus are incomplete for the Ancestral wave.*

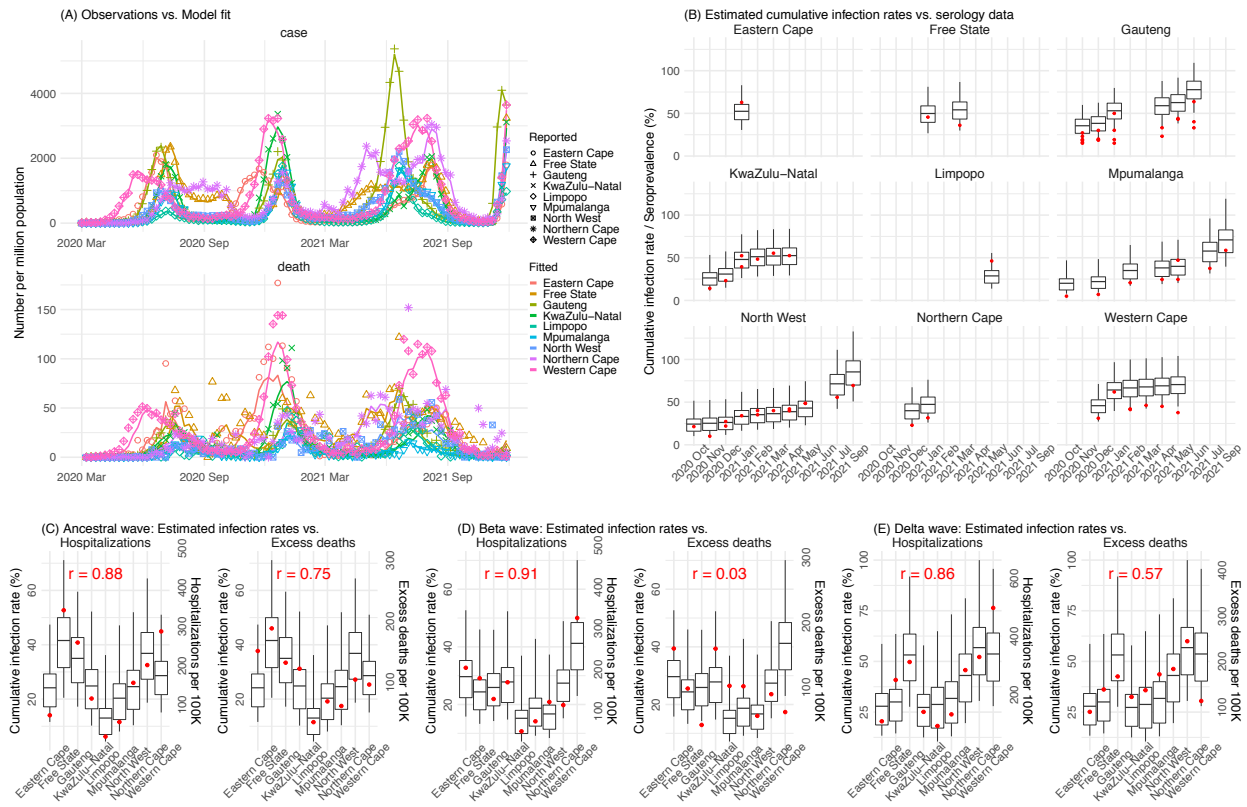


Fig 2. Example model-inference estimates for Gauteng. (A) Observed relative mobility, vaccination rate, and estimated disease seasonal trend, compared to case and death rates over time. Key model-inference estimates are shown for the time-varying effective reproduction number R_t (B), transmissibility (C), population susceptibility (D), infection-detection rate (E), and infection-fatality risk (F). Grey shaded areas indicate the approximate circulation period for each variant. In (B) – (F), blue lines and surrounding areas show the estimated mean, 50% (dark) and 95% (light) CrIs; boxes and whiskers show the estimated mean, 50% and 95% CrIs for estimated infection rates. *Note that the transmissibility estimates (in C) have removed the effects of changing population susceptibility, NPIs, and disease seasonality; thus, the trends are more stable than the reproduction number (R_t in B) and reflect changes in variant-specific properties. Also note that infection-fatality risk estimates were based on reported COVID-19 deaths and may not reflect true values due to likely under-reporting of COVID-19 deaths.*

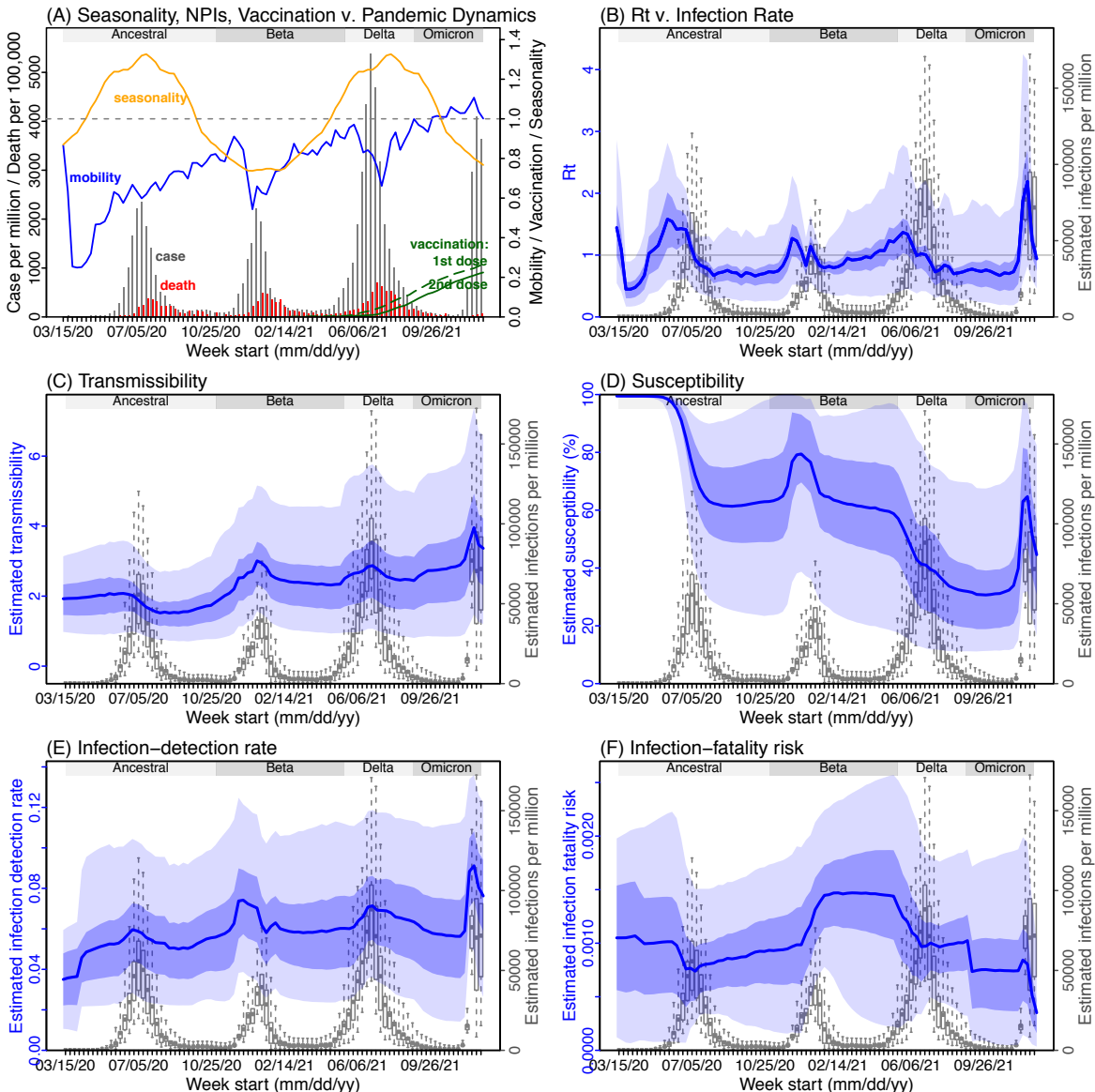
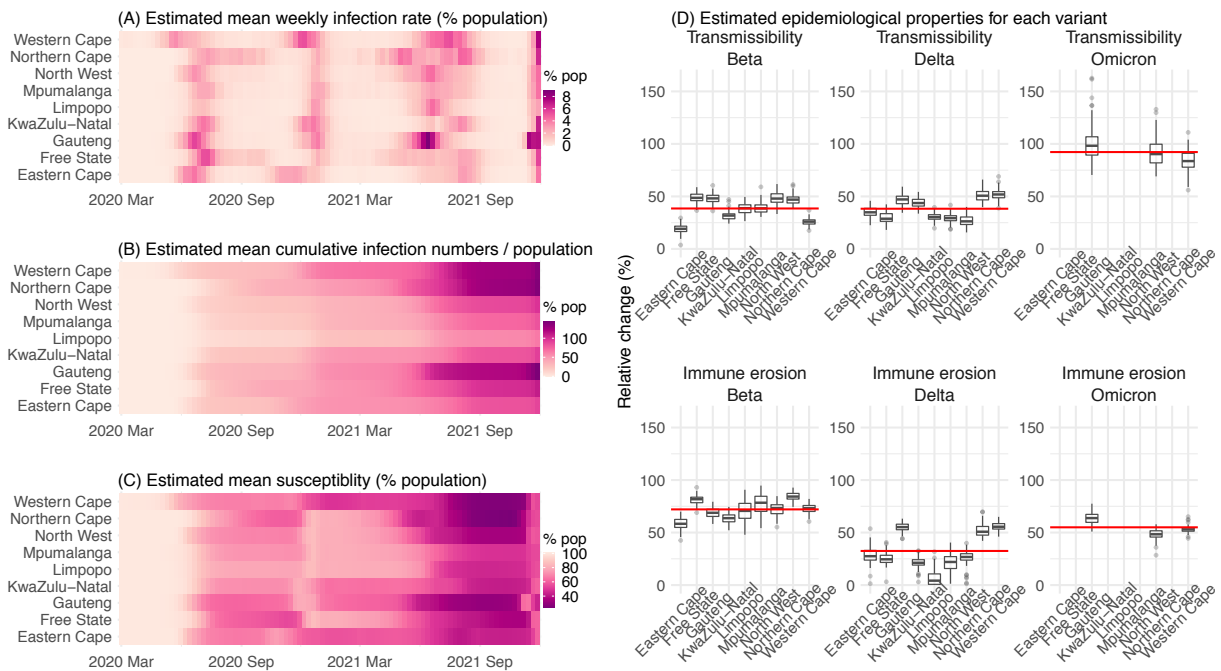


Fig 3. Model-inferred epidemiological properties for different variants across SA provinces. Heatmaps show (A) Estimated mean infection rates by week (x-axis) and province (y-axis), (B) Estimated mean *cumulative* infection numbers relative to the population size in each province, and (C) Estimated population susceptibility (to the circulating variant) by week and province. (D) Boxplots in the top row show the estimated distribution of changes in transmissibility for Beta, Delta, and Omicron, relative to the Ancestral SARS-CoV-2, for each province (middle bar = median; edges = 50% CIs; and whiskers = 95% CIs); boxplots in the bottom row show, for each variant, the estimated distribution of immune erosion to all adaptive immunity gained from infection and vaccination prior to that variant. Red lines show the mean across all provinces. Estimates for Omicron are not shown for some provinces, as data were not sufficient for model inference.



Supplemental Figures and Tables

Fig S1. Model-fit to case and death data in each province. Dots show reported SARS-CoV-2 cases and deaths by week. Blue lines and surrounding area show model estimated median, 50% (darker blue) and 95% (lighter blue) credible intervals.

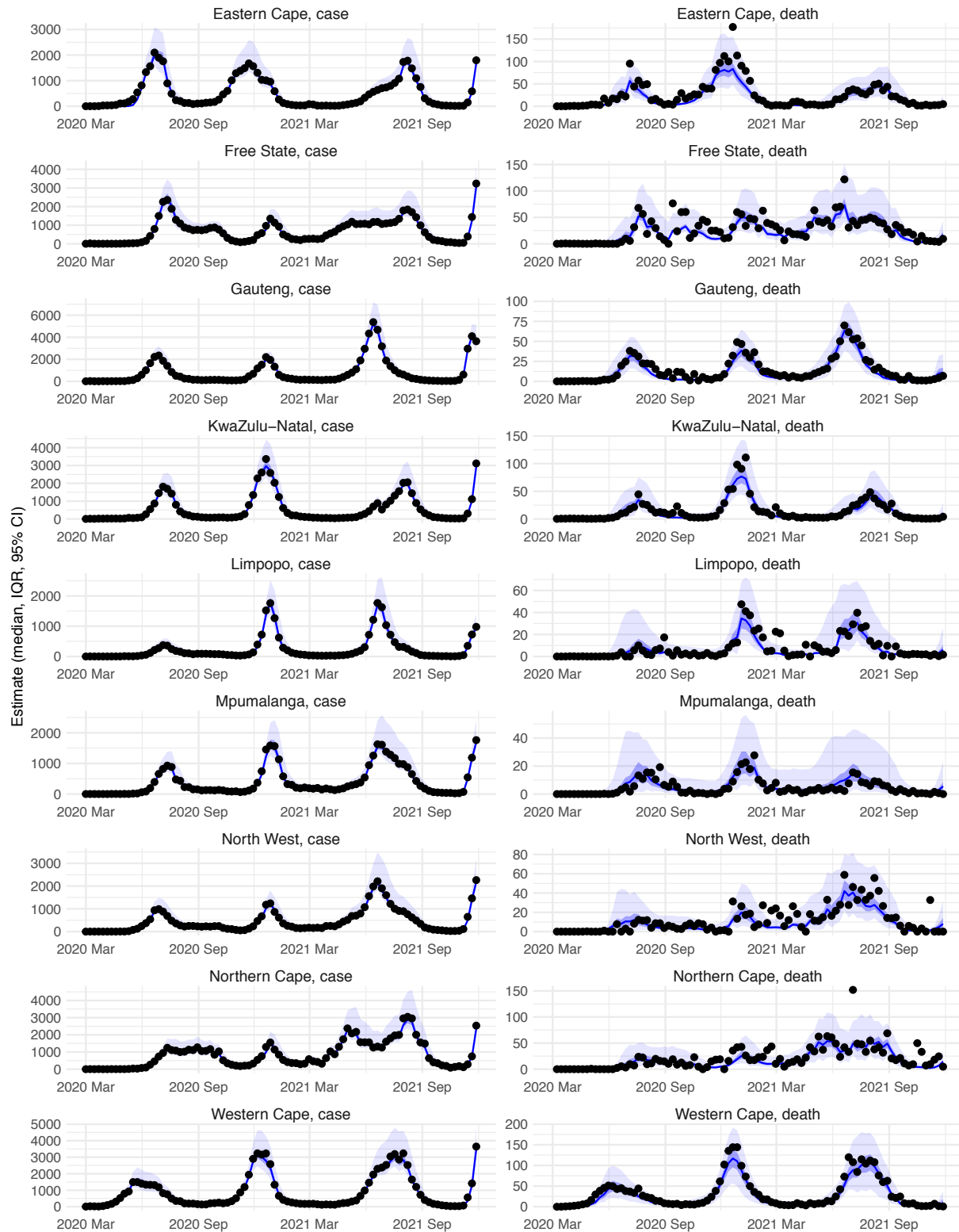


Fig S2. Model inference estimates for Eastern Cape. (A) Observed relative mobility, vaccination rate, and estimated disease seasonal trend, compared to case and death rates over time. Key model-inference estimates are shown for the time-varying effective reproduction number R_t (B), transmissibility (C), population susceptibility (D), infection-detection rate (E), and infection-fatality risk (F). Grey shaded areas indicate the approximate circulation period for each variant. In (B) – (F), blue lines and surrounding areas show the estimated mean, 50% (dark) and 95% (light) CrIs; boxes and whiskers show the estimated mean, 50% and 95% CrIs for estimated infection rates. *Note that the transmissibility estimates (in C) have removed the effects of changing population susceptibility, NPIs, and disease seasonality; thus, the trends are more stable than the reproduction number (R_t in B) and reflect changes in variant-specific properties.* Also note that infection-fatality risk estimates were based on reported COVID-19 deaths and may not reflect true values due to likely under-reporting of COVID-19 deaths.

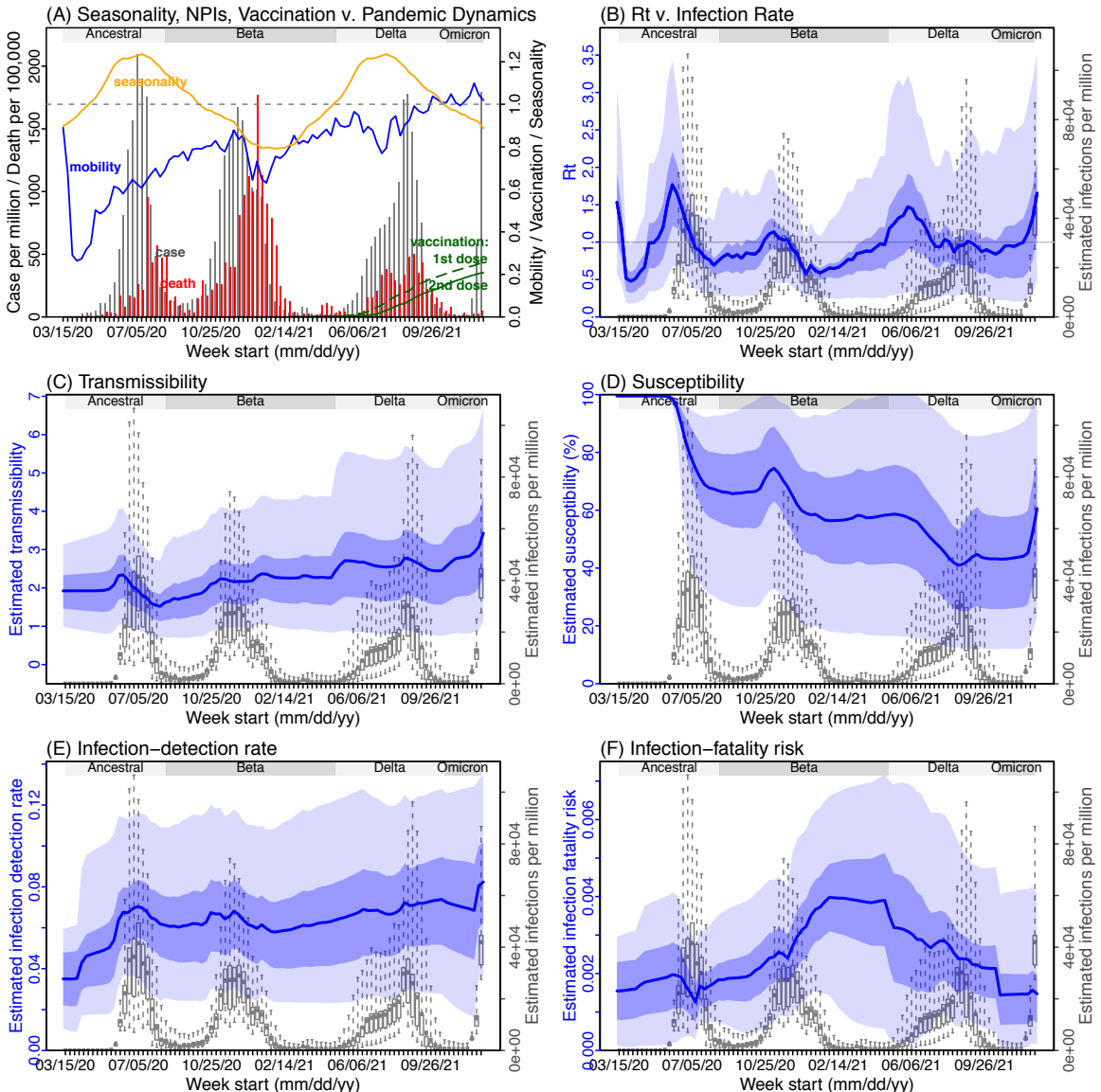


Fig S3. Model inference estimates for Free State. (A) Observed relative mobility, vaccination rate, and estimated disease seasonal trend, compared to case and death rates over time. Key model-inference estimates are shown for the time-varying effective reproduction number R_t (B), transmissibility (C), population susceptibility (D), infection-detection rate (E), and infection-fatality risk (F). Grey shaded areas indicate the approximate circulation period for each variant. In (B) – (F), blue lines and surrounding areas show the estimated mean, 50% (dark) and 95% (light) CrIs; boxes and whiskers show the estimated mean, 50% and 95% CrIs for estimated infection rates. *Note that the transmissibility estimates (in C) have removed the effects of changing population susceptibility, NPIs, and disease seasonality; thus, the trends are more stable than the reproduction number (R_t in B) and reflect changes in variant-specific properties.* Also note that infection-fatality risk estimates were based on reported COVID-19 deaths and may not reflect true values due to likely under-reporting of COVID-19 deaths.

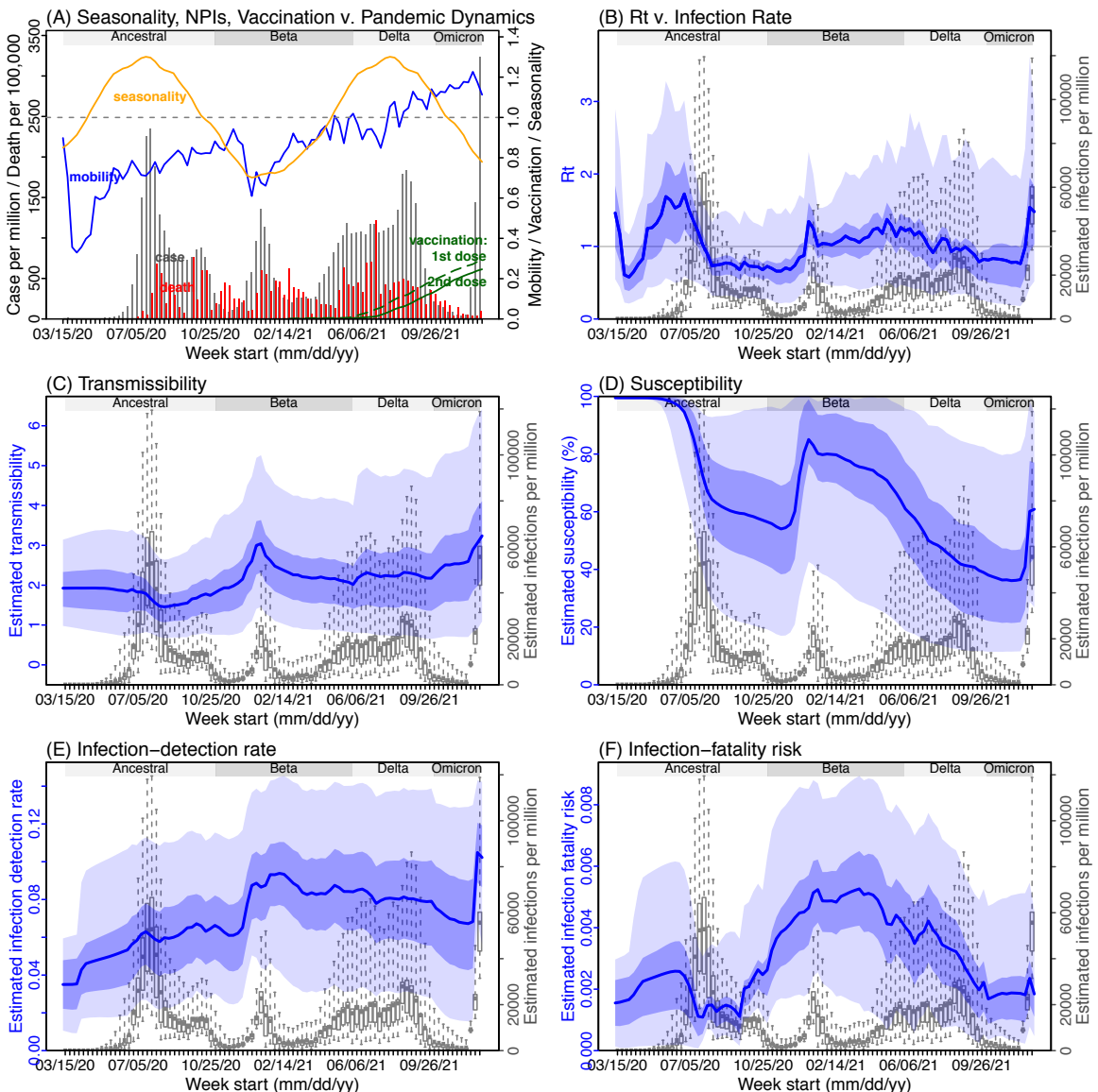


Fig S4. Model inference estimates for *KwaZulu-Natal*. (A) Observed relative mobility, vaccination rate, and estimated disease seasonal trend, compared to case and death rates over time. Key model-inference estimates are shown for the time-varying effective reproduction number R_t (B), transmissibility (C), population susceptibility (D), infection-detection rate (E), and infection-fatality risk (F). Grey shaded areas indicate the approximate circulation period for each variant. In (B) – (F), blue lines and surrounding areas show the estimated mean, 50% (dark) and 95% (light) CrIs; boxes and whiskers show the estimated mean, 50% and 95% CrIs for estimated infection rates. *Note that the transmissibility estimates (in C) have removed the effects of changing population susceptibility, NPIs, and disease seasonality; thus, the trends are more stable than the reproduction number (R_t in B) and reflect changes in variant-specific properties. Also note that infection-fatality risk estimates were based on reported COVID-19 deaths and may not reflect true values due to likely under-reporting of COVID-19 deaths.*

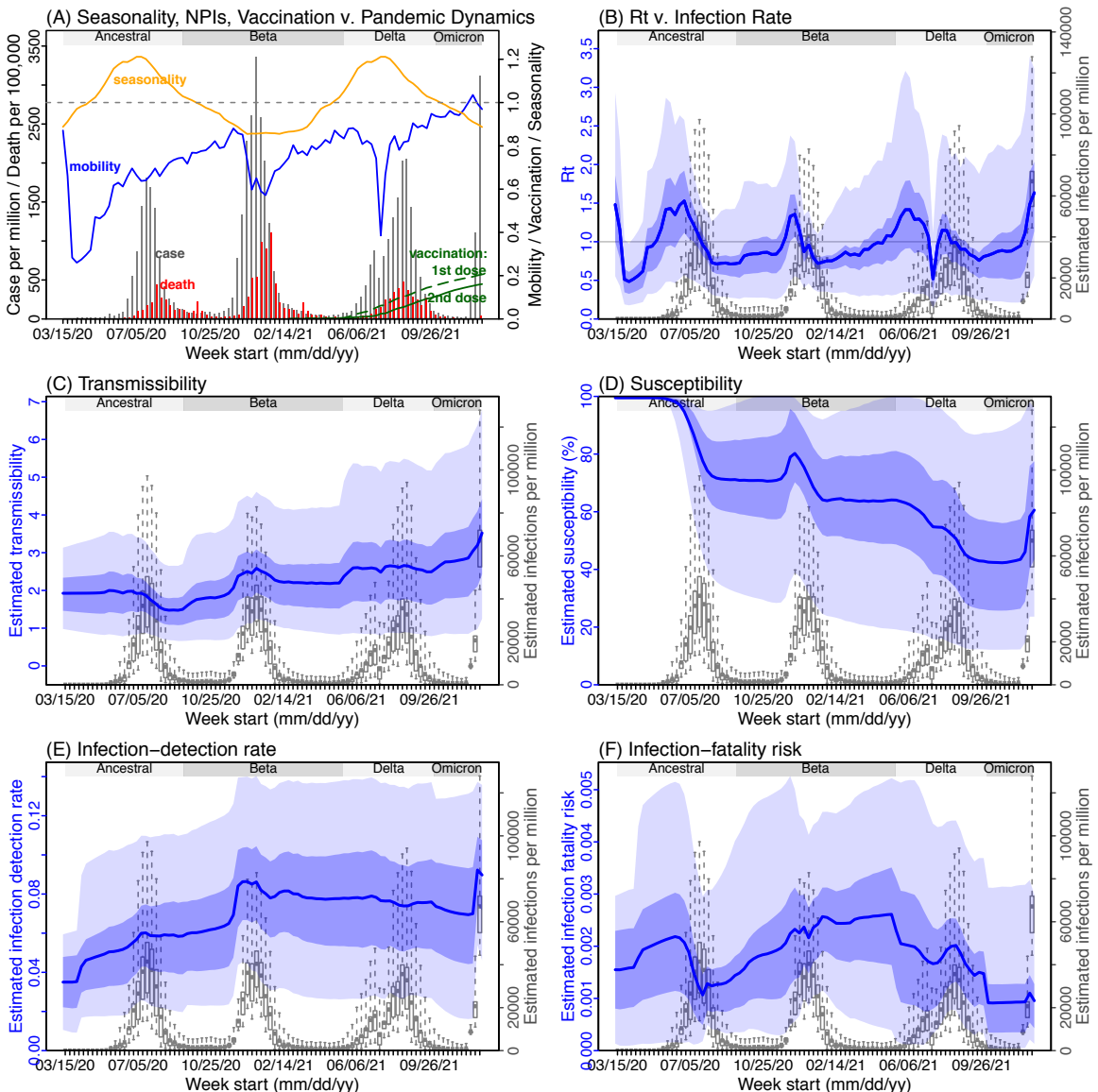


Fig S5. Model inference estimates for Limpopo. (A) Observed relative mobility, vaccination rate, and estimated disease seasonal trend, compared to case and death rates over time. Key model-inference estimates are shown for the time-varying effective reproduction number R_t (B), transmissibility (C), population susceptibility (D), infection-detection rate (E), and infection-fatality risk (F). Grey shaded areas indicate the approximate circulation period for each variant. In (B) – (F), blue lines and surrounding areas show the estimated mean, 50% (dark) and 95% (light) CrIs; boxes and whiskers show the estimated mean, 50% and 95% CrIs for estimated infection rates. *Note that the transmissibility estimates (in C) have removed the effects of changing population susceptibility, NPIs, and disease seasonality; thus, the trends are more stable than the reproduction number (R_t in B) and reflect changes in variant-specific properties.* Also note that infection-fatality risk estimates were based on reported COVID-19 deaths and may not reflect true values due to likely under-reporting of COVID-19 deaths.

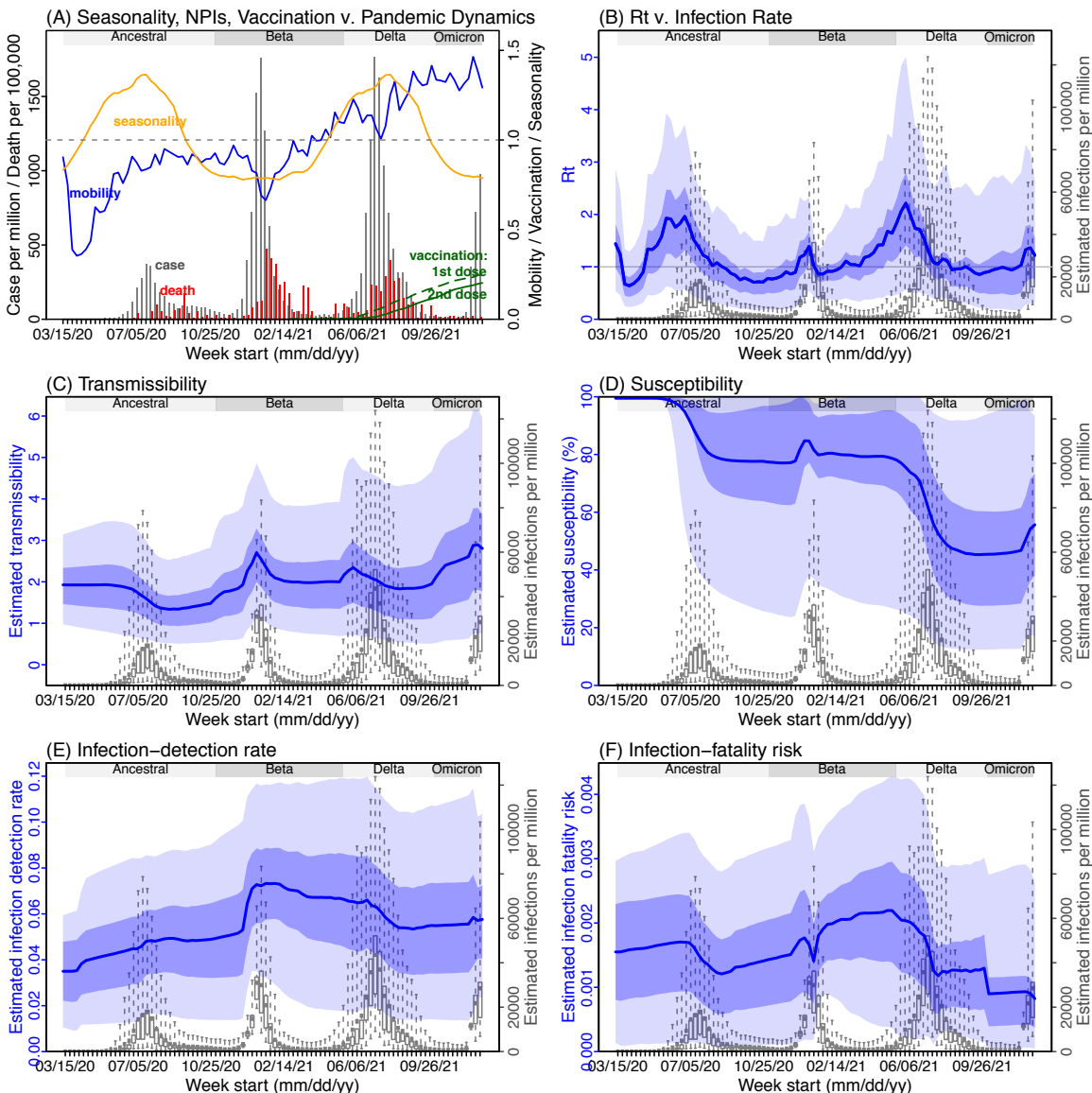


Fig S6. Model inference estimates for Mpumalanga. (A) Observed relative mobility, vaccination rate, and estimated disease seasonal trend, compared to case and death rates over time. Key model-inference estimates are shown for the time-varying effective reproduction number R_t (B), transmissibility (C), population susceptibility (D), infection-detection rate (E), and infection-fatality risk (F). Grey shaded areas indicate the approximate circulation period for each variant. In (B) – (F), blue lines and surrounding areas show the estimated mean, 50% (dark) and 95% (light) Crls; boxes and whiskers show the estimated mean, 50% and 95% Crls for estimated infection rates. *Note that the transmissibility estimates (in C) have removed the effects of changing population susceptibility, NPIs, and disease seasonality; thus, the trends are more stable than the reproduction number (R_t in B) and reflect changes in variant-specific properties. Also note that infection-fatality risk estimates were based on reported COVID-19 deaths and may not reflect true values due to likely under-reporting of COVID-19 deaths.*

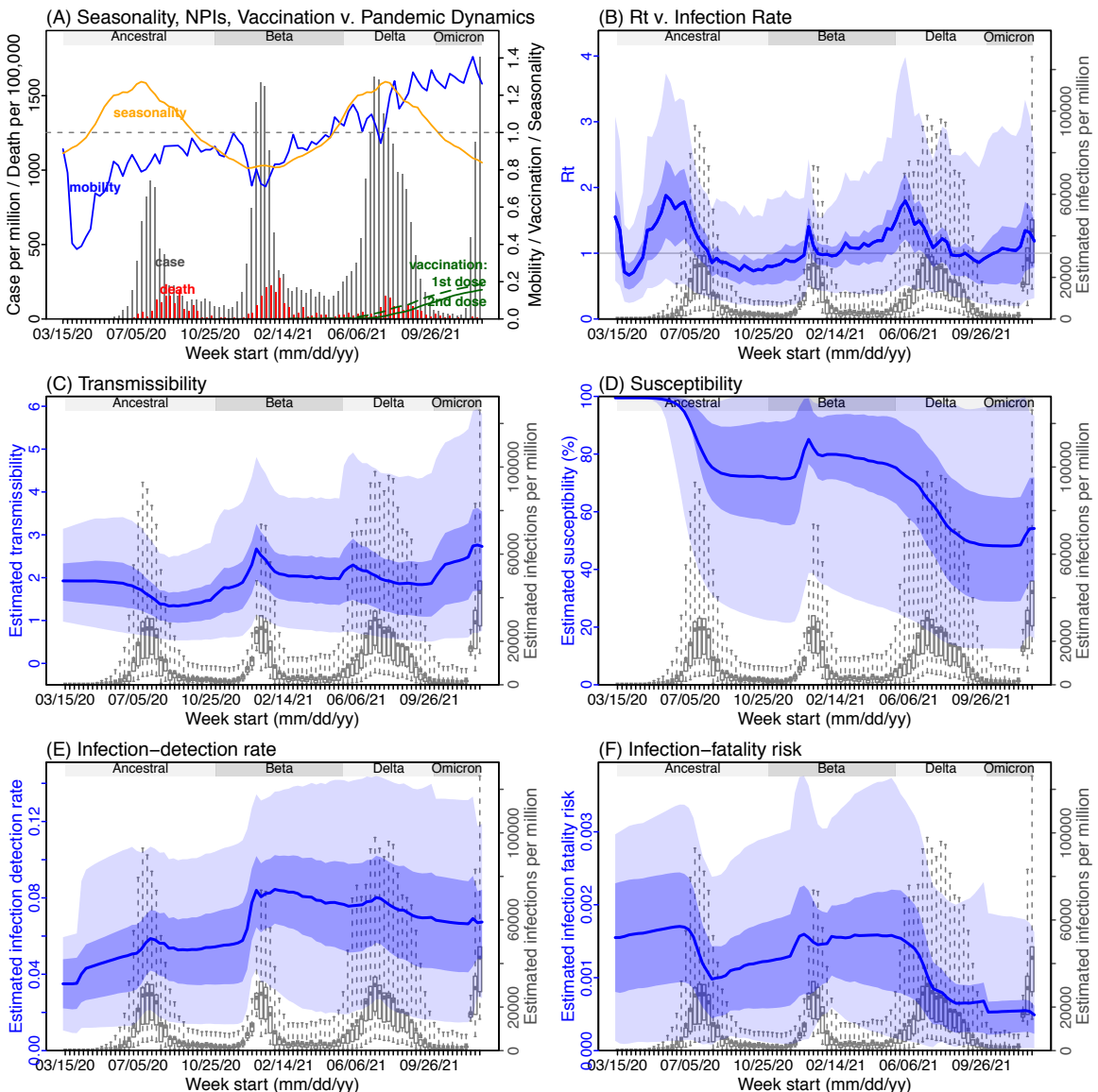


Fig S7. Model inference estimates for North West. (A) Observed relative mobility, vaccination rate, and estimated disease seasonal trend, compared to case and death rates over time. Key model-inference estimates are shown for the time-varying effective reproduction number R_t (B), transmissibility (C), population susceptibility (D), infection-detection rate (E), and infection-fatality risk (F). Grey shaded areas indicate the approximate circulation period for each variant. In (B) – (F), blue lines and surrounding areas show the estimated mean, 50% (dark) and 95% (light) CrIs; boxes and whiskers show the estimated mean, 50% and 95% CrIs for estimated infection rates. *Note that the transmissibility estimates (in C) have removed the effects of changing population susceptibility, NPIs, and disease seasonality; thus, the trends are more stable than the reproduction number (R_t in B) and reflect changes in variant-specific properties.* Also note that infection-fatality risk estimates were based on reported COVID-19 deaths and may not reflect true values due to likely under-reporting of COVID-19 deaths.

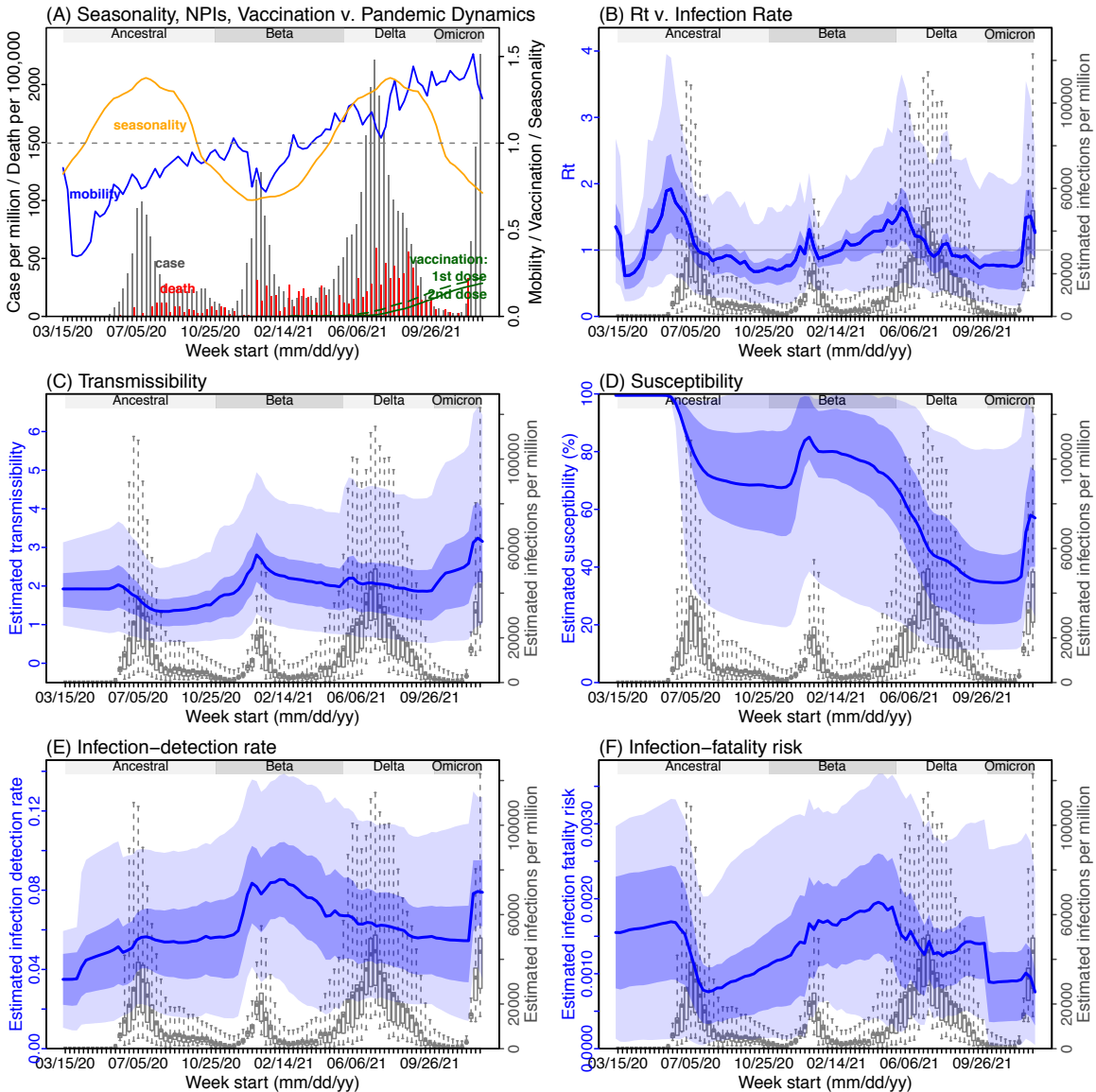


Fig S8. Model inference estimates for Northern Cape. (A) Observed relative mobility, vaccination rate, and estimated disease seasonal trend, compared to case and death rates over time. Key model-inference estimates are shown for the time-varying effective reproduction number R_t (B), transmissibility (C), population susceptibility (D), infection-detection rate (E), and infection-fatality risk (F). Grey shaded areas indicate the approximate circulation period for each variant. In (B) – (F), blue lines and surrounding areas show the estimated mean, 50% (dark) and 95% (light) CrIs; boxes and whiskers show the estimated mean, 50% and 95% CrIs for estimated infection rates. *Note that the transmissibility estimates (in C) have removed the effects of changing population susceptibility, NPIs, and disease seasonality; thus, the trends are more stable than the reproduction number (R_t in B) and reflect changes in variant-specific properties. Also note that infection-fatality risk estimates were based on reported COVID-19 deaths and may not reflect true values due to likely under-reporting of COVID-19 deaths.*

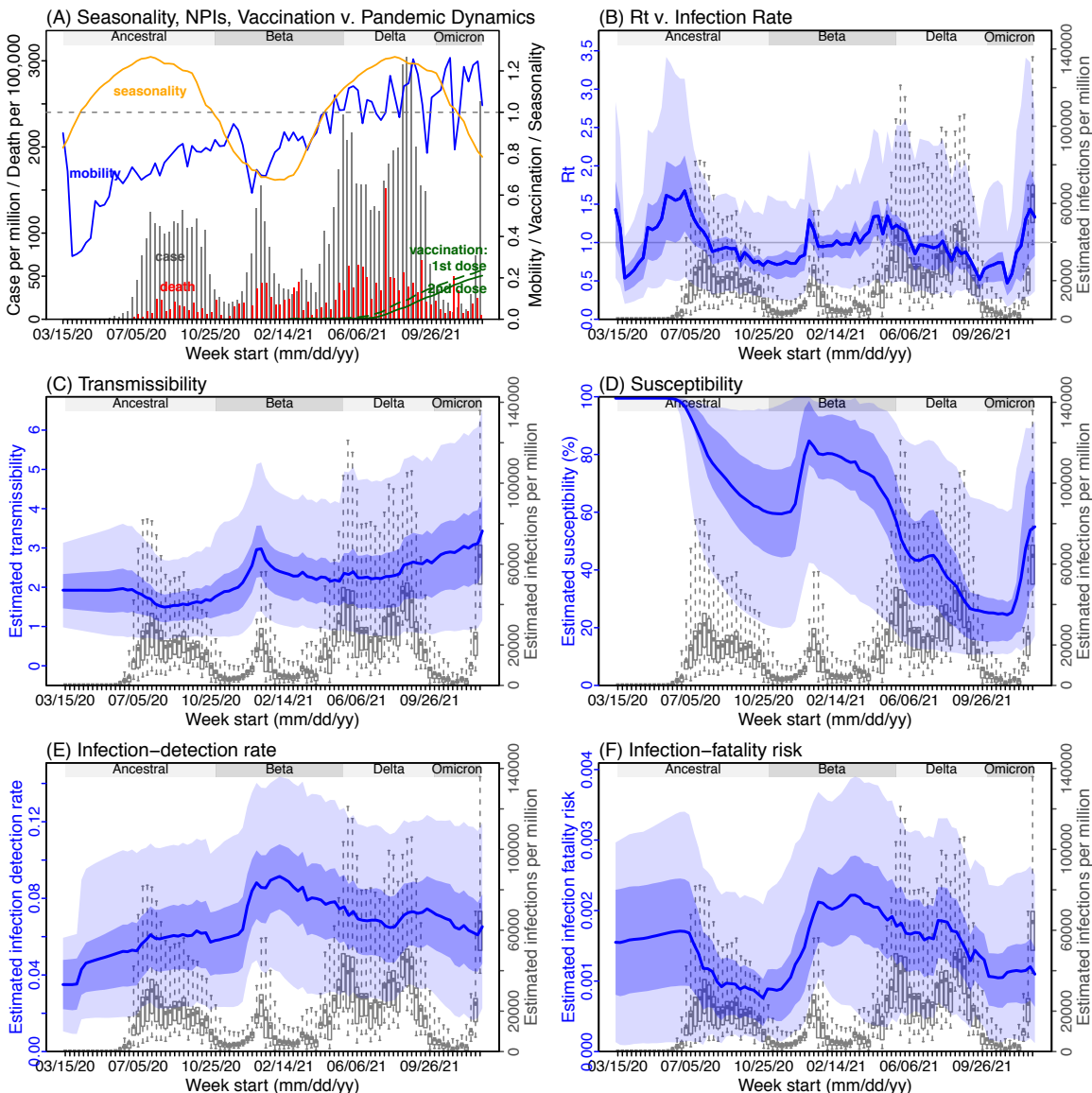


Fig S9. Model inference estimates for Western Cape. (A) Observed relative mobility, vaccination rate, and estimated disease seasonal trend, compared to case and death rates over time. Key model-inference estimates are shown for the time-varying effective reproduction number R_t (B), transmissibility (C), population susceptibility (D), infection-detection rate (E), and infection-fatality risk (F). Grey shaded areas indicate the approximate circulation period for each variant. In (B) – (F), blue lines and surrounding areas show the estimated mean, 50% (dark) and 95% (light) Crls; boxes and whiskers show the estimated mean, 50% and 95% Crls for estimated infection rates. *Note that the transmissibility estimates (in C) have removed the effects of changing population susceptibility, NPIs, and disease seasonality; thus, the trends are more stable than the reproduction number (R_t in B) and reflect changes in variant-specific properties. Also note that infection-fatality risk estimates were based on reported COVID-19 deaths and may not reflect true values due to likely under-reporting of COVID-19 deaths.*

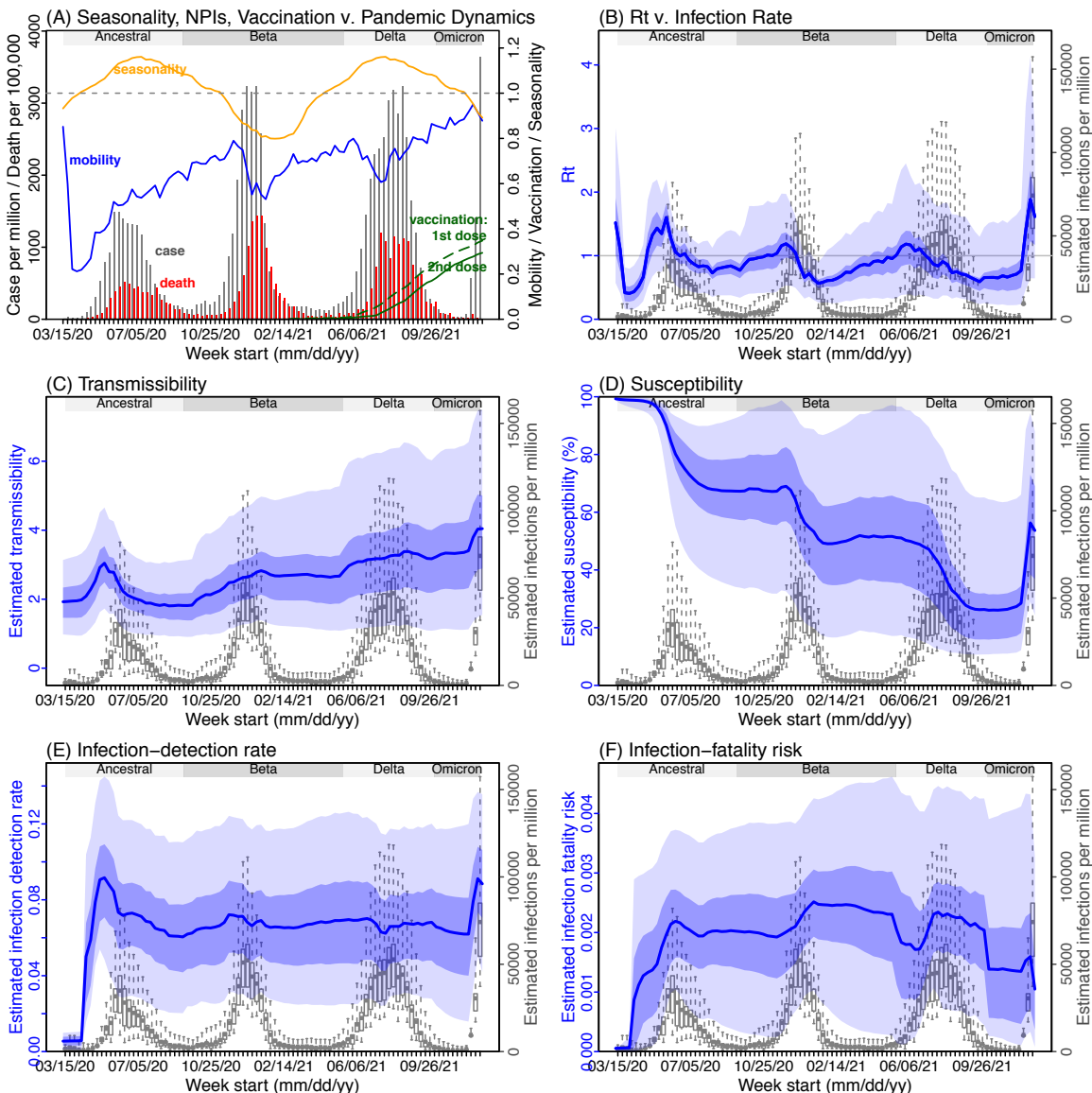


Table S1. Model estimated infection-detection rate during each wave. Numbers show the estimated percentage of infections (including asymptomatic and subclinical infections) documented as cases (mean and 95% CI in parentheses).

Province	Ancestral wave	Beta wave	Delta wave
Eastern Cape	5.16 (2.63, 10.74)	5.65 (3.18, 10.6)	5.12 (2.43, 10.69)
Free State	4.74 (2.77, 9.62)	6.65 (3.52, 12.2)	6.69 (3.16, 13.86)
Gauteng	4.31 (2.53, 8.75)	5.21 (2.94, 9.47)	5.88 (3.4, 11.32)
KwaZulu-Natal	4.19 (1.99, 10.16)	7.01 (3.73, 13.21)	5.66 (2.67, 12.39)
Limpopo	2.26 (0.81, 6.69)	5.15 (2.12, 10.94)	3.34 (1.48, 9.18)
Mpumalanga	3.19 (1.38, 8.04)	5.82 (2.54, 11.88)	4.89 (2.12, 11.91)
North West	3.37 (1.59, 7.96)	5.55 (2.49, 11.11)	4.55 (2.41, 10.01)
Northern Cape	4.71 (2.69, 9.28)	6.38 (3.58, 11.5)	6.54 (3.67, 12.19)
Western Cape	5.58 (3.13, 10.59)	6.39 (3.76, 11.47)	6.01 (3.37, 11.56)

Table S2. Model estimated attack rate during each wave. Numbers show estimated cumulative infection numbers, expressed as percentage of population size (mean and 95% CI in parentheses).

Province	Ancestral wave	Beta wave	Delta wave
Eastern Cape	24.17 (11.61, 47.43)	29.66 (15.81, 52.7)	27.88 (13.36, 58.64)
Free State	41.57 (20.5, 71.16)	24.37 (13.29, 46.02)	30 (14.47, 63.54)
Gauteng	34.99 (17.22, 59.52)	25.91 (14.26, 45.91)	53.19 (27.61, 91.87)
KwaZulu-Natal	24.84 (10.25, 52.22)	27.83 (14.78, 52.35)	27.3 (12.47, 57.92)
Limpopo	13.03 (4.39, 36.21)	15.21 (7.15, 36.94)	28.77 (10.47, 64.91)
Mpumalanga	20.34 (8.08, 47.13)	18.7 (9.16, 42.77)	31.74 (13.02, 73.22)
North West	24.59 (10.39, 51.98)	16.73 (8.37, 37.32)	43.06 (19.56, 81.15)
Northern Cape	36.83 (18.69, 64.41)	27.41 (15.22, 48.93)	56.81 (30.5, 101.16)
Western Cape	28.64 (15.09, 51.06)	41.21 (22.96, 70.11)	53.67 (27.93, 95.67)

Table S3. Model estimated infection-fatality risk during each wave. Numbers are percentages (%; mean and 95% CI in parentheses). Note that these estimates were based on reported COVID-19 deaths and may be biased due to likely under-reporting of COVID-19 deaths.

Province	Ancestral wave	Beta wave	Delta wave
Eastern Cape	0.15 (0.08, 0.31)	0.46 (0.26, 0.86)	0.19 (0.09, 0.39)
Free State	0.13 (0.07, 0.25)	0.42 (0.22, 0.76)	0.27 (0.13, 0.55)
Gauteng	0.09 (0.05, 0.18)	0.16 (0.09, 0.28)	0.1 (0.06, 0.19)
KwaZulu-Natal	0.09 (0.04, 0.22)	0.25 (0.13, 0.47)	0.14 (0.06, 0.3)
Limpopo	0.06 (0.02, 0.17)	0.21 (0.08, 0.44)	0.1 (0.04, 0.27)
Mpumalanga	0.06 (0.03, 0.16)	0.09 (0.04, 0.19)	0.04 (0.02, 0.09)
North West	0.05 (0.02, 0.11)	0.2 (0.09, 0.4)	0.14 (0.07, 0.3)
Northern Cape	0.06 (0.03, 0.11)	0.21 (0.12, 0.37)	0.17 (0.09, 0.31)
Western Cape	0.21 (0.12, 0.4)	0.27 (0.16, 0.48)	0.22 (0.12, 0.42)

Table S4. Prior ranges for the parameters used in the model-inference system.

Parameter/ variable	Symbol	Prior range	Source/rationale
Initial exposed	$E(t=0)$	1 – 100 times of reported cases during the Week of March 15, 2020 for Western Cape; 1 – 10 times of reported cases during the Week of March 15, 2020, for other provinces	Low infection-detection rate in first weeks; earlier and higher case numbers reported in Western Cape than other provinces.
Initial infectious	$I(t=0)$	Same as for $E(t=0)$	
Initial susceptible	$S(t=0)$	99 – 100% of the population	Almost everyone is susceptible initially
Population size	N	N/A	Based on population data from COVID19ZA (main text ref 24)
Variant-specific transmission rate	β	For all provinces, starting from U[0.4, 0.7] at time 0 and allowed to increase over time using space re-probing ⁵ with values drawn from U[0.5, 0.9] during the Beta wave, U[0.7, 1.25] during the Delta wave, and U[0.7, 1.3] during the Omicron wave.	For the initial range at model initialization, based on R_0 estimates of around 1.5-4 for SARS-CoV-2. ¹⁻³ For the Beta, Delta and Omicron variants, we use large bounds for space re-probing (SR) ⁵ to explore the parameter state space and enable estimation of changes in transmissibility due to the new variants. Note that SR is only applied to 3-10% of the ensemble members and β can migrate outside either the initial range or the SR ranges during EAKF update.
Scaling of effectiveness of NPI	e	[0.5, 1.5], for all provinces	Around 1, with a large bound to be flexible.

Latency period	Z	[2, 5] days, for all provinces	Incubation period: 5.2 days (95% CI: 4.1, 7) ¹ ; latency period is likely shorter than the incubation period
Infectious period	D	[2, 5] days, for all provinces	Time from symptom onset to hospitalization: 3.8 days (95% CI: 0, 12.0) in China, ⁴ plus 1-2 days viral shedding before symptom onset. We did not distinguish symptomatic/asymptomatic infections.
Immunity period	L	[730, 1095] days, for all provinces	Assuming immunity lasts for 2-3 years
Mean of time from viral shedding to diagnosis	T_m	[5, 8] days, for all provinces	From a few days to a week from symptom onset to diagnosis/reporting, ⁴ plus 1-2 days of viral shedding (being infectious) before symptom onset.
Standard deviation (SD) of time from viral shedding to diagnosis	T_{sd}	[1, 3] days, for all provinces	To allow variation in time to diagnosis/reporting
Infection-detection rate	r	<u>For Western Cape</u> : starting from U[0.001, 0.01] at time 0 and allowed to increase over time using space re-probing ⁵ with values drawn from U[0.02, 0.1] during 4/19/- 9/15/20 (Ancestral wave), U[0.02, 0.12] during the Beta wave (9/16/20 – 5/15/21), U[0.03, 0.12] during the Delta wave	Large uncertainties; therefore, in general we use large prior bounds and large bounds for space re-probing (SR). Note that SR is only applied to 3-10% of the ensemble members and r can migrate

Infection fatality risk (IFR)	<p>(5/16/21 – 9/30/21), and U[0.01, 0.08] starting 10/1/21 (Omicron wave).</p> <p><u>For Limpopo and Mpumalanga:</u> starting from U[0.01, 0.06] at time 0 and allowed to increase over time using space re-probing⁵ with values drawn from U[0.01, 0.08] for Limpopo and U[0.01, 0.1] for Mpumalanga during 4/12/2020 - 10/31/20 (Ancestral wave), U[0.01, 0.1] during the Beta wave (11/1/20 – 5/15/21), U[0.01, 0.1] during the Delta wave (5/16/21 – 9/30/21), and U[0.01, 0.08] starting 10/1/21 (Omicron wave).</p> <p><u>For Other provinces:</u> starting from U[0.01, 0.06] at time 0 and allowed to increase over time using space re-probing⁵ with values drawn from U[0.02, 0.1] starting 4/12/2020 for the rest of Ancestral wave, U[0.02, 0.12] during the Beta wave, U[0.03, 0.12] during the Delta wave, and U[0.01, 0.08] starting 10/1/21 (Omicron wave).</p> <p><u>For Western Cape:</u> starting from U[0.00001, 0.0001] at time 0 and allowed to change over time using space re-probing⁵ with values drawn from U[0.00001, 0.0003] during 3/16/20 – 4/11/20, U[0.00001, 0.003] during 4/12/20 – 5/15/21 (Ancestral wave and Beta wave), U[0.00001, 0.0015] during 5/16/21 – 9/30/21 (Delta wave) and U[0.00001, 0.00075] starting 10/1/21 (Omicron wave).</p> <p><u>For Gauteng:</u> starting from [0.0001, 0.002] at time 0 and allowed to change over time using space re-probing⁵ with values drawn from U[0.0001, 0.0015] during 4/19/2020 - 12/12/2020, values drawn from U[0.0001, 0.002] during 12/13/2020 – 5/15/21 (due to Beta), U[0.0001, 0.0015] during the Delta wave, and U[0.00001, 0.00075] starting 9/1/21 (Omicron wave).</p>	<p>outside either the initial range or the SR ranges during EAKF update.</p> <p>Western Cape had earlier and higher case numbers during March – April 2020 than other provinces, suggesting lower detection rate at the time.</p> <p>Lower case rates in Limpopo and Mpumalanga, suggesting likely lower detection rate; thus, we used slightly lower numbers for space-reprobing in these two provinces</p> <p>Based on previous estimates⁶ but extend to have wider ranges. Note that SR is only applied to 3-10% of the ensemble members and IFR can migrate outside either the initial range or the SR ranges during EAKF update.</p> <p>Western Cape had earlier and higher case numbers during March – April 2020 than other provinces, suggesting lower detection rate at the time.</p> <p>Initial mortality rate in Gauteng was relatively low because initial infections occurred mainly among middle-aged, returning holiday makers.⁷</p>
-------------------------------	---	---

For Limpopo and Mpumalanga: starting from $U[0.0001, 0.003]$ at time 0 and allowed to change over time using space re-probing⁵ with values drawn from $U[0.0001, 0.004]$ during the Beta wave, $U[0.0001, 0.003]$ during the Delta wave, $U[0.00001, .001]$ for Limpopo and $U[0.00001, 0.00075]$ for Mpumalanga starting 10/1/21 (Omicron wave).

For Eastern Cape: starting from $U[0.0001, 0.003]$ at time 0 and allowed to change over time using space re-probing⁵ with values drawn from $U[0.0001, 0.004]$ during 4/19/20 – 12/1/20 (Ancestral wave and earlier phase of Beta wave), $U[0.0001, 0.006]$ during 12/2/20 – 4/30/21 (the Beta wave), $[0.0001, 0.003]$ during the Delta wave, and $U[0.00001, 0.0015]$ or starting 10/16/21 (Omicron wave).

For KwaZulu-Natal: starting from $U[0.0001, 0.003]$ at time 0 and allowed to change over time using space re-probing⁵ with values drawn from $U[0.0001, 0.005]$ during 4/19/20 – 5/15/21 (ancestral wave and Beta wave), $U[0.0001, 0.0015]$ during the Delta wave, and $U[0.00001, 0.00075]$ starting 10/1/21 (Omicron wave).

For Northern Cape: starting from $U[0.0001, 0.003]$ at time 0 and allowed to change over time using space re-probing⁵ with values drawn from $U[0.00001, 0.0015]$ starting 10/1/21 (Omicron wave).

For Free State: starting from $U[0.0001, 0.003]$ at time 0 and allowed to change over time using space re-probing⁵ with values drawn from $U[0.0001, 0.006]$ during 3/16/20 – 10/31/20, $U[0.0001, 0.008]$ during the Beta and Delta waves, and $U[0.00001, 0.0015]$ starting 10/1/21 (Omicron wave).

Earlier spread of Beta in Eastern Cape, KwaZulu-Natal, and Northern Cape, higher numbers of deaths per capita reported. Free State reported higher number of deaths per capita.

References including in Table S4:

- 1 Li, Q. *et al.* Early Transmission Dynamics in Wuhan, China, of Novel Coronavirus–Infected Pneumonia. *New Engl J Med*, doi:10.1056/NEJMoa2001316 (2020).
- 2 Wu, J. T., Leung, K. & Leung, G. M. Nowcasting and forecasting the potential domestic and international spread of the 2019-nCoV outbreak originating in Wuhan, China: a modelling study. *Lancet*, doi:10.1016/S0140-6736(20)30260-9 (2020).
- 3 Li, R. *et al.* Substantial undocumented infection facilitates the rapid dissemination of novel coronavirus (SARS-CoV-2). *Science* **368**, 489-493, doi:10.1126/science.abb3221 (2020).
- 4 Zhang, J. *et al.* Evolving epidemiology and transmission dynamics of coronavirus disease 2019 outside Hubei province, China: a descriptive and modelling study. *The Lancet. Infectious diseases*, doi:10.1016/S1473-3099(20)30230-9 (2020).
- 5 Yang, W. & Shaman, J. A simple modification for improving inference of non-linear dynamical systems. *arXiv*, 1403.6804 (2014).
- 6 Verity, R. *et al.* Estimates of the severity of coronavirus disease 2019: a model-based analysis. *The Lancet. Infectious diseases*, doi:10.1016/S1473-3099(20)30243-7 (2020).
- 7 Giandhari, J. *et al.* Early transmission of SARS-CoV-2 in South Africa: An epidemiological and phylogenetic report. *Int J Infect Dis* **103**, 234-241, doi:10.1016/j.ijid.2020.11.128 (2021).

Table S5. Approximate epidemic timing for each wave in each province.

Province	Variant	Start date	End date
Eastern Cape	Ancestral	3/15/20	8/15/20
Eastern Cape	Beta	8/16/20	4/30/21
Eastern Cape	Delta	5/1/21	10/15/21
Eastern Cape	Omicron	10/16/21	NA
Free State	Ancestral	3/15/20	10/31/20
Free State	Beta	11/1/20	5/31/21
Free State	Delta	6/1/21	9/30/21
Free State	Omicron	10/1/21	NA
Gauteng	Ancestral	3/15/20	10/31/20
Gauteng	Beta	11/1/20	5/15/21
Gauteng	Delta	5/16/21	8/31/21
Gauteng	Omicron	9/1/21	NA
KwaZulu-Natal	Ancestral	3/15/20	9/15/20
KwaZulu-Natal	Beta	9/16/20	5/15/21
KwaZulu-Natal	Delta	5/16/21	9/30/21
KwaZulu-Natal	Omicron	10/1/21	NA
Limpopo	Ancestral	3/15/20	10/31/20
Limpopo	Beta	11/1/20	5/15/21
Limpopo	Delta	5/16/21	9/30/21
Limpopo	Omicron	10/1/21	NA
Mpumalanga	Ancestral	3/15/20	10/31/20
Mpumalanga	Beta	11/1/20	5/15/21
Mpumalanga	Delta	5/16/21	9/30/21
Mpumalanga	Omicron	10/1/21	NA
North West	Ancestral	3/15/20	10/31/20
North West	Beta	11/1/20	5/15/21
North West	Delta	5/16/21	9/30/21
North West	Omicron	10/1/21	NA
Northern Cape	Ancestral	3/15/20	10/31/20
Northern Cape	Beta	11/1/20	5/15/21
Northern Cape	Delta	5/16/21	9/30/21
Northern Cape	Omicron	10/1/21	NA
Western Cape	Ancestral	3/15/20	9/15/20
Western Cape	Beta	9/16/20	5/15/21
Western Cape	Delta	5/16/21	9/30/21
Western Cape	Omicron	10/1/21	NA